Chapter 5
Multiple UAV Formation Control

Haibin Duan

Abstract Formation flight has long been performed by many species of birds for its social and aerodynamic benefits. As a challenging interdisciplinary research topic, autonomous formation flight for multiple unmanned aerial vehicles (UAVs) is about flying in formations with precisely defined geometries, with the benefits of fuel saving and improved efficiency in air traffic control and cooperative task allocation. This chapter mainly focuses on three important aspects associated with formation, which are respectively formation control, close formation (tight formation), and formation configuration. A chaotic particle swarm optimization (PSO)-based nonlinear dual-mode receding horizon control (RHC) method is proposed to cope with the complexity and nonlinearity of vehicle dynamics. Then a novel type of control strategy of using hybrid RHC and differential evolution (DE) algorithm is proposed based on the nonlinear model of multiple UAV close formation. Moreover, based on the Markov chain model, the convergence of DE is proved. Finally, the formation configuration, which is about diving multiple UAVs to form a new flying formation state, is explained in detail using the RHC-based DE. The global control problem of multiple UAV formation reconfiguration is transformed into several online local optimization problems at a series of receding horizons, while the DE algorithm is adopted to optimize control sequences at each receding horizon.

5.1 Introduction

Unmanned aerial vehicle (UAV), which develops in the direction of unmanned attendance and intelligence, is small in size, is light in weight, is low cost, and is able to operate autonomously. With these qualities, UAV has become one of the inevitable trends of the modern military and civilian applications. Recently there has been a considerable amount of interests in cooperative control of a group of UAVs flying in a formation. When multiple UAVs fly in formation, the formation's initial

---

The original version of this chapter was revised. A correction to this chapter is available at https://doi.org/10.1007/978-3-642-41196-0__9

DOI 10.1007/978-3-642-41196-0_5, © Springer-Verlag Berlin Heidelberg 2014

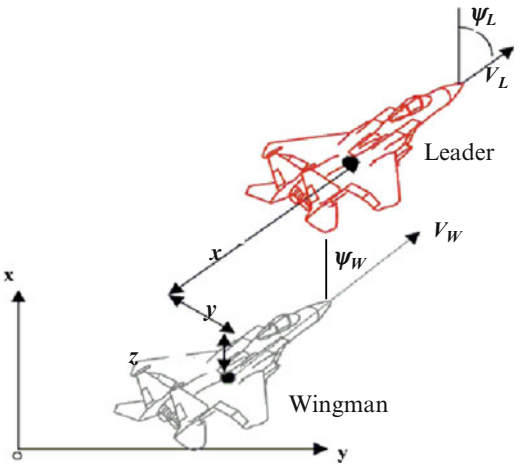

Fig. 5.1 Leader–Wingman formation (Reprinted from Zhang et al. (2010), with kind permission from Springer Science+Business Media)

geometry, including the longitudinal, lateral, and vertical separation, should be preserved during maneuvers with heading change, speed change, and altitude change.

5.1.1 Formation Control

In recent years, formation control of multiple UAVs has become a challenging interdisciplinary research topic, while autonomous formation flight is an important research area in the aerospace field (Duan et al. 2013a). The main motivation is the wide range of military and civilian applications where UAVs formations could provide a low-cost and efficient alternative to existing technology. Multiple UAV teams flying in formations with precisely defined geometries have many advantages, such as energy saving when the vortex forces are taken into account. Formation flight can also be used for airborne refueling and quick deployment of troops and vehicles. Formation flight can be regarded as a complicated control problem which computes the inputs driving the UAVs along challenging maneuvers while maintaining relative positions as well as safe distances between each UAV pair (Duan et al. 2013b). The challenge here lies in designing a formation controller that is computationally simple yet robust.

5.1.2 Close Formation

A close formation, also called "tight formation," is one in which "the lateral separation between UAV is less than a wingspan" (Pachter et al. 2001). In this case, aerodynamic coupling is introduced into the formation's dynamics. Multiple UAVs flying in a close formation can achieve a significant reduction in power demand, thereby improving cruise performances, such as range and speed, or to increase the payload (Binetti et al. 2003). The "Leader–Wingman" formation pattern can be shown with Fig. 5.1. If the Wingman flies in close formation with the leading UAV,

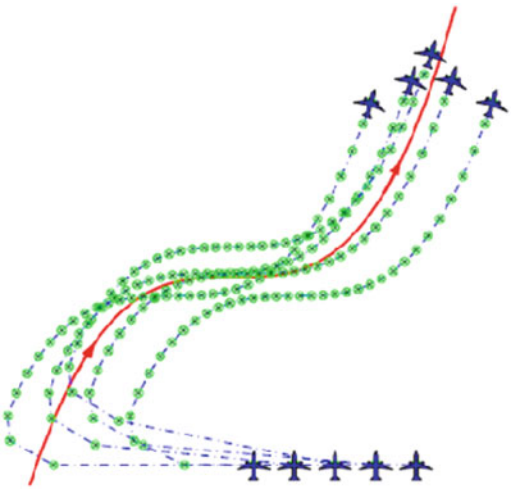

Fig. 5.2 Formation reconfiguration of five UAVs (Reprinted from Zhang and Duan (2012), with kind permission from SAGE Publications)

the Leader's vortices will produce aerodynamic coupling effects, and a reduction in the formation's drag can be achieved. According to the effects of aerodynamic interference, multiple UAV close formation flight control is a complex problem with strongly nonlinear and coupling character.

5.1.3 Formation Configuration

The formation reconfiguration problem for multiple UAVs can be described as follows: given a group of UAVs with an initial configuration, a final configuration, and a set of inter- and intra-UAV constraints, the goal is to determine a nominal control input for each vehicle such that the multiple UAV group can start from the initial configuration and reach its final configuration while satisfying the set of constraints, as is shown in Fig. 5.2. The formation reconfiguration problem can be recognized as an optimal control problem with dynamic constraints (Zelinski et al. 2003; Ueno and Kwon 2007; Duan et al. 2008). Several theoretical techniques such as graph theory (Hendrickx et al. 2008), reconfiguration maps, Dijkstra algorithm (Giulietti et al. 2000), or functional optimization have been developed to define the new/optimal positions to be occupied by the UAVs in the formation.

As a large-scale centralized control problem, formation reconfiguration aims to obtain the control input signals (such as steering angle, throttle/thrust) for each UAV through complex calculation to drive each UAV in a complicated flight maneuver. In this process, multiple UAVs must satisfy several constraints; for example, the distance between two UAVs must be greater than the safety collision distance, and also should not be too greater than the communication distance.

5.2 Dual-Mode RHC for Multiple UAV Formation Flight Based on Chaotic PSO

5.2.1 *Leader-Following Formation Model*

The point mass model is considered for formation flight. Each UAV is assumed to fly at a constant altitude, parallel to the 2-dimensional region to be surveyed. A commonly used nonlinear kinematics model that represents a UAV with zero or negligible velocity in the direction perpendicular to the UAV's heading is applied to our model.

$$\begin{aligned} \dot{x} &= v\cos\psi \\ \dot{y} &= v\sin\psi \\ \dot{v} &= u \\ \dot{\psi} &= \omega \end{aligned} \tag{5.1}$$

where x and y are the Cartesian coordinates of the UAV, v is the velocity, and ψ is the heading angle in the (x,y) plan (Stipanović et al. 2004). The acceleration in the longitudinal direction u and angular turn rate ω are assumed to be the control inputs to the UAV. Figure 5.3 shows the UAV position and orientation in the plane coordinate system.

In a typical multiple UAV formation flight, the Wingman follows the trajectory of the Leader UAV, taking other aircrafts as reference to keep its own position inside the formation. In a large formation, intra-aircraft distances must be kept constant (Giulietti et al. 2000). The formation model in this paper adopts Leader mode strategy (as shown in Fig. 5.4), which means each Wingman UAV takes its trajectory references from the Leader UAV, while the altitude is the same for all. The Leader UAV takes charge of formation trajectory.

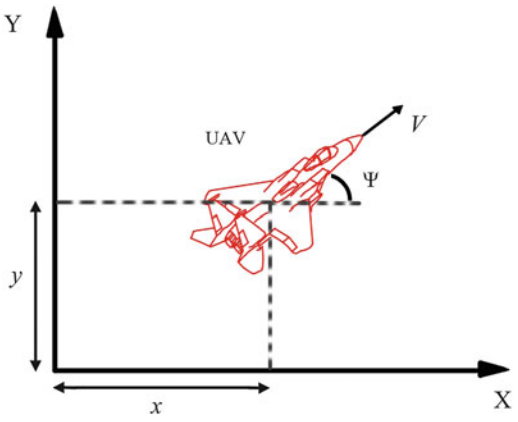

Fig. 5.3 UAV position and orientation (© [2002] IEEE. Reprinted, with permission, from Duan and Liu (2010))

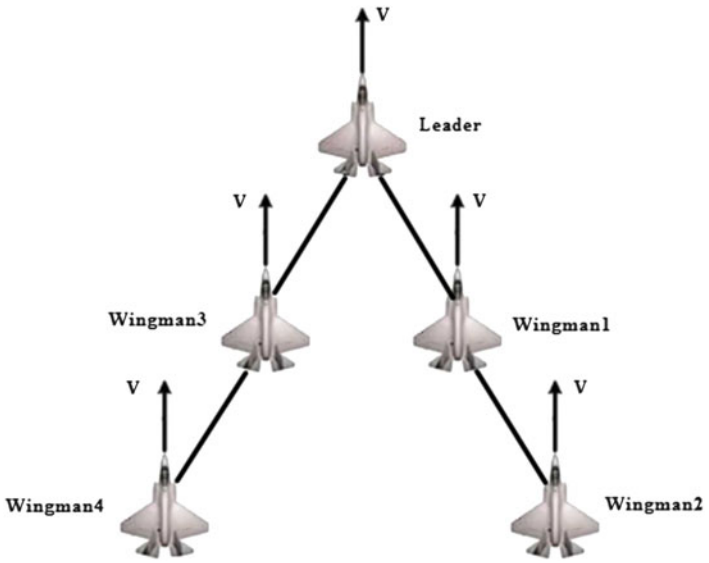

Fig. 5.4 Multiple UAV formation (© [2002] IEEE. Reprinted, with permission, from Duan and Liu (2010))

The Virtual Leader is employed in our model to replace the real UAV Leader so that UAVs adjust speed and heading angle based on the relative states of Virtual Leader (as shown in Fig. 5.5). Then a multiple UAV formation, defined with respect to all the real UAVs as well as to the Virtual Leader, should be maintained at the same time as the Virtual Leader tracks its reference trajectory. The key advantage of the Virtual Leader UAV is that a physical UAV Leader is subject to destruction, while the Virtual Leader can never be damaged. The Virtual Leader provides a stabile, robust reference for formation control.

5.2.2 Principle of RHC

Nonlinear RHC is that the finite time optimal control law is computed by solving an online optimization problem. And linear RHC theory is quite mature so far (Kwon and Han 2005). Generally, many systems are inherently nonlinear, and they are often required to operate over a wide range of operating conditions. Linear models are often inadequate to describe the process dynamics, and nonlinear models have to be used. This motivates the use of nonlinear RHC. The optimization problems over the finite horizon, on which the RHC is based, can be applied to a broad class of

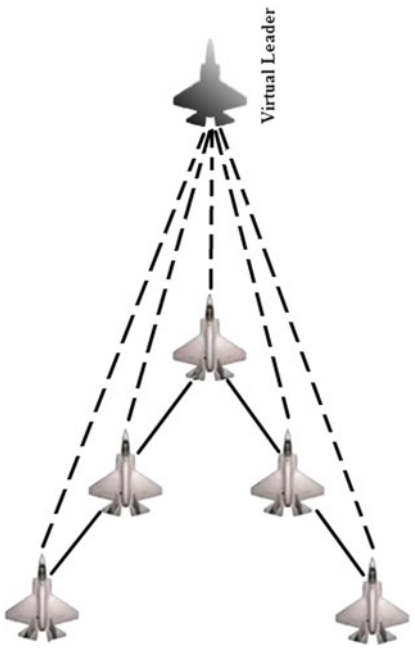

Fig. 5.5 Multiple UAV formation with the Virtual Leader (© [2002] IEEE. Reprinted, with permission, from Duan and Liu (2010))

systems, including nonlinear systems and time-delayed systems. Thus, the RHC has the same broad applications even for nonlinear systems:

$$\begin{aligned} &\min_{u} J = f\left(x, u; t_c, T_p\right) \\ &J = \int_{t_c}^{t_c+T_p} F\left(x, u\right) dt + \Phi\left(x_{t_c+T_p}\right) \\ &\textit{subject to } \dot{x} = f\left(x, u\right) \\ &L \leq \begin{bmatrix} x \\ u \end{bmatrix} \leq U \end{aligned} \tag{5.2}$$

where x and u are respectively state vector and control sequence; t_c and T_p represent the control and the prediction horizon with $t_c \leq T_p$; L and U are lower and upper bounds; and δ is the predicted time step.

Receding optimization is the most important idea of RHC, which is also the typical difference between RHC and optimum control, as shown in Fig. 5.6 (Duan and Liu 2010; Zhang et al. 2011; Duan et al. 2011). The whole control process can be divided into a series of optimizing intervals called rolling window or receding horizon. RHC method forms the closed-loop rolling mechanism, including observation, planning, implementation, and reobservation. RHC is a p -step-ahead online optimization strategy. At each time interval, RHC optimizes the specific problem for the following p intervals based on current available information.

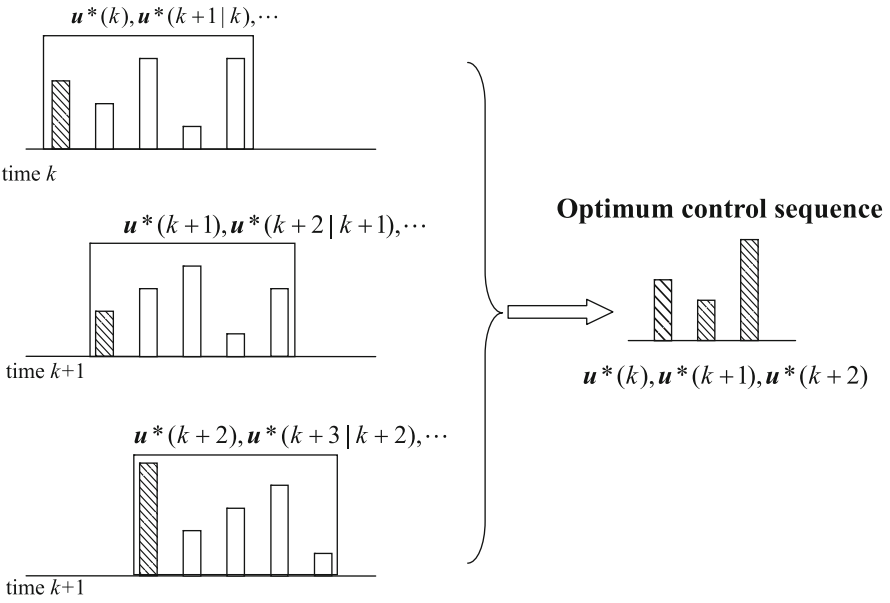

Fig. 5.6 Receding optimization (Reprinted from Zhang et al. (2010), with kind permission from Springer Science+Business Media)

5.2.3 Chaotic PSO-Based Dual-Mode RHC Formation Controller Design

5.2.3.1 A Dual-Mode Formation Controller Design

In this subsection, we will introduce the framework of the multiple UAV formation flight controller (Duan and Liu 2010). In our proposed formation flight control strategy, each UAV follows the Virtual UAV Leader.

The *i*th UAV state vector and control input sequence in (5.1) are

$$\boldsymbol{x}_i = (v_i, \Psi_i, x_i, y_i), \boldsymbol{u}_i = (u_i, \omega_i) \tag{5.3}$$

The Virtual Leader state is $\boldsymbol{x}_{VL}$ and control inputs are $\boldsymbol{u}_{VL}$. According to the UAV Leader, the *i*th UAV relative state is $\boldsymbol{x}_{ri} = \boldsymbol{x}_i - \boldsymbol{x}_{VL}$. We define formation state and input sequence:

$$X = (\boldsymbol{x}_{VL}, \boldsymbol{x}_1, \ldots, \boldsymbol{x}_N), X_r = (\boldsymbol{x}_{r1}, \ldots, \boldsymbol{x}_{rN}), U = (\boldsymbol{u}_{VL}, \boldsymbol{u}_1, \ldots, \boldsymbol{u}_N) \tag{5.4}$$

In nonlinear RHC, the input applied to the system is usually given by the solution of the following finite horizon optimal control problem according to (5.2), which is solved at every sampling instant:

$$
\begin{aligned}
J &= \min_{U} \int_{t}^{t+T_p} \mathrm{F}\left(X_r(\tau), U(\tau)\right) d\tau + \mathrm{V}\left(X_r\left(t+T_p\right)\right) \\
s.t.\ \dot{X}(\tau) &= \mathrm{f}(X(\tau), U(\tau)) \\
U(\tau) &\in U \forall \tau \in [t, t+t_c] \\
X(\tau) &\in X \forall \tau \in \left[t, t+T_p\right] \\
X\left(t+T_p\right) &\in \Omega
\end{aligned} \tag{5.5}
$$

where

$$
F\left(X_r, U\right) = {X_r}^T Q X_r + U^T R U \tag{5.6}
$$

$$
V\left(X_r\left(t+T_p\right)\right) = X\left(t+T_p\right)_r{}^T P X\left(t+T_p\right)_r \tag{5.7}
$$

The deviation from the desired values is weighted by the positive-definite matrices Q, R, and P; the time step is δ. V is the terminal penalty.

$$
\boldsymbol{\Omega} = \left\{X \left| X^T P X \le \alpha \right.\right\} \tag{5.8}
$$

The terminal region $\boldsymbol{\Omega}$ is chosen such that it is invariant for the nonlinear system control by using a linear state feedback. As control systems become more complex and performance requirements more demanding, the invariant sets are widely employed to design stabilizing controllers and, in particular, for applying RHC strategies. In order to enlarge the solution range and make search process of PSO easier, the dual-mode control strategy is chosen in this paper, for this strategy provides an efficient way to guarantee the stability of RHC with input constraints. The basic idea is to use a finite horizon of allowable control inputs to steer the state into an invariant set. The terminal region $\boldsymbol{\Omega}$ and terminal penalty matrix P can be determined off-line.

A local linear control law which stabilizes the nonlinear system in $\boldsymbol{\Omega}$ is obtained as follows:

$$
\dot{X} = \frac{\partial f}{\partial x}(0,0)\, X + \frac{\partial f}{\partial u}(0,0)\, u \tag{5.9}
$$

Substitute the linear state feedback $u = KX$ into (5.9), we can get

$$
\dot{X} = \boldsymbol{f}\, X \tag{5.10}
$$

$$
\boldsymbol{f} = \frac{\partial f}{\partial x}(0,0) + \frac{\partial f}{\partial u}(0,0)\, K \tag{5.11}
$$

Define the following Lyapunov equation:

$$
\boldsymbol{f}\, P + P\, \boldsymbol{f}^T + Q^* = 0 \tag{5.12}
$$

where $Q^* = Q + K^T RK$ and the solution P is a positive-definite symmetric matrix. For any vector $X \in R^n$, $\|X\|$ denotes Euclidean norm. There exists a constant $\alpha \in (0,\infty)$ to fix the terminal region $\boldsymbol{\Omega}$ at the origin as (5.8). The constant α satisfies $KX \in \boldsymbol{U}$ for all $x \in \boldsymbol{\Omega}$ and the following condition, according to (5.8) and $u = KX$:

$$\begin{aligned} \|KX\| &= \left\| K\left(\alpha^{\frac{1}{2}} P^{-\frac{1}{2}}\right)\left(\alpha^{-\frac{1}{2}} P^{\frac{1}{2}} X\right)\right\| \le \left\| K\left(\alpha^{\frac{1}{2}} P^{-\frac{1}{2}}\right)\right\| \cdot \left\|\alpha^{-\frac{1}{2}} P^{\frac{1}{2}} X\right\| \\ &\le \left\| K\alpha^{\frac{1}{2}} P^{-\frac{1}{2}}\right\| = \alpha K^T PK \end{aligned} \tag{5.13}$$

It follows the input constraints that

$$\alpha K^T PK \le u_{\max}^2 \ \|u\| \le u_{\max} \tag{5.14}$$

As multiple UAV formation state X enter the terminal region $\boldsymbol{\Omega}$, X will be kept in this region all the while and tend to the origin gradually.

5.2.3.2 Collision Avoidance

In multiple UAV formation flight system, each UAV moves in an environment in which there are obstacles and other UAVs. Thus the multiple UAVs, at the same time, have to consider the problem of formation control and collisions avoidance. Collision avoidance is assumed to be the most important task: only when UAV is at safe distance from the other UAVs and the obstacles can it take care of maintaining the formation.

To achieve collision avoidance with other UAVs, a priority indexing scheme is used (Wang et al. 2007): all UAVs are tagged, and the UAV with a lower index creates an imaginary obstacle around the UAV with a higher index (as seen in Fig. 5.7) and tries to avoid it. Thus, collision avoidance is achieved.

The UAVs with a lower index must react rapidly when neighboring UAVs with a higher index approach within unsafe range or when obstacles are detected as they appear within the sensor range, to avoid any collision. Consequently, a multiple UAV formation control strategy that ensures avoidance of collisions is achieved by adding a constraint to (5.5).

$$J_1 = J + Penalty_c \cdot \sum_{j=1}^{Co_{num}} Dis_{\text{constraint}}\left(d_{ij}\right) \tag{5.15}$$

$$Dis_{\text{constraint}}\left(d_{ij}\right) = \begin{cases} 1 & d_{ij} \le d_{safe} \\ 0 & d_{ij} > d_{safe} \end{cases} \tag{5.16}$$

where $Penalty_c$ is the collision penalty coefficient, Co_{num} is the total account of collisions that UAV_i has to avoid, and d_{ij} is the distance between UAV_i and the jth collision center. (The obstacle shape is specified as a circle.) As long as UAV_i spatial

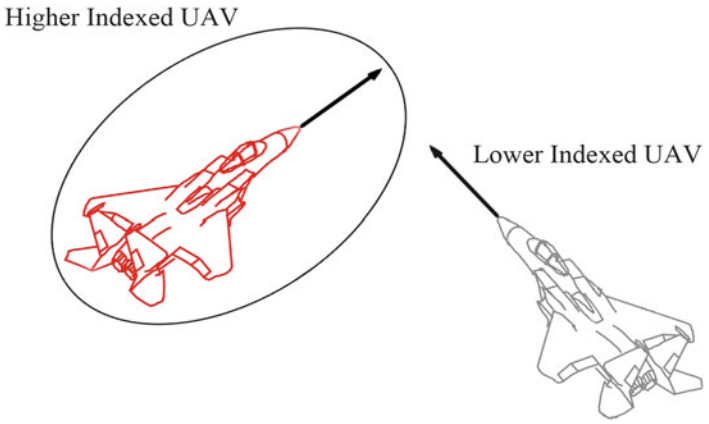

Fig. 5.7 Collision avoidance (© [2002] IEEE. Reprinted, with permission, from Duan and Liu (2010))

horizon overlaps the *j*th obstacle, $Dis_{constra\,\mathrm{int}}(d_{ij}) = 1$ and the value of (5.15) will be very large. Therefore, this constraint is adopted for effectively avoiding collisions.

5.2.3.3 Chaotic Particle Swarm Optimization

In RHC, the cost function (5.15) plays a role of an evaluation function in PSO. The future control input sequence U is obtained by minimizing (5.15) via a particle swarm optimization.

In PSO design, the optimization concepts based on chaotic sequences can be a good alternative to provide diversity in PSO populations. The application of chaotic sequences instead of random sequences in PSO is a powerful strategy to diversify the population of particles and improve the PSO's performance in preventing premature convergence to local minimum. Chaos optimization is realized through chaos variables which can be obtained by many ways. One of the simplest maps which is brought to the attention of scientists by May (1976), which appears in nonlinear dynamics of biological population evidencing chaotic behavior, is logistic map:

$$Z_{n+1} = \mu Z_n (1 - Z_n) \tag{5.17}$$

where Z_n is the nth chaotic number where n denotes the iteration number. Obviously, $Z_n \in (0,1)$ under the conditions that the initial $Z_0 \in (0,1)$, and $Z_n \notin \{0.0,0.25,0.5,0.75,1.0\}$. $\mu = 4$ has been used in our algorithm.

The population diversity measured the average particle distance, which describes population diversity with dispersion degree between particles. Assume L is the maximum length of search space, ps is the population of particles, `ln` is the

dimensions of solution space, p_{id} is the dth coordinate of particle p_i, P_d is the average of the dth coordinate, and the average particles distance $D(iter_k)$ at the kth iteration is defined as follows:

$$D\left(iter_k\right) = \frac{1}{ps \cdot L} \sum_{i}^{ps} \sqrt{\sum_{d=1}^{ln} \left(p_{id} - P_d\right)^2} \tag{5.18}$$

In our chaotic PSO approach, the PSO algorithm is first run to find the global-best position as a candidate solution, and once particles collide, $D(iter_k) < \varepsilon$, where ε is a positive constant. Then, the better solution generated from chaotic systems substitute random numbers for the PSO particles, where it is necessary to make a random-based choice. In this way, the global convergence can be improved, and falling into local-best solution can be prevented.

As we have mentioned, PSO can also be improved by a modification of the inertia weight w in (2.11) (Shi and Eberhart 1998). The inertia weight can be used to balance the local and global search during the optimization process. If the inertia weight is big, it is possible to enhance global search. Otherwise, smaller inertia weight will enhance the local search. While the value of w is made to decrease gradually with the increase in the number of iterations by the following equation at the kth iteration $iter_k$:

$$w = w_{\max} - iter_k \frac{w_{\max} - w_{\min}}{iter_{\max}} \tag{5.19}$$

where $iter_{\max}$ is maximum iteration and $w_{\max}$ and $w_{\min}$ are separately maximum and minimum of w.

In order to guarantee the stability and enhance the efficiency of the control algorithm, the initial value of each particle chooses the last control input sequence after the achievement of primary sequence, such as the lth particle at a time t is initialed by $U(t-\delta)$.

The process of our proposed nonlinear dual-mode RHC method based on chaotic PSO for solving multiple UAV formation flight problem can be described as follows:

Step 1. Initialize UAVs states X_0 and the nonlinear dual-mode RHC parameters used in formation system.

Step 2. Evaluate the terminal region $\boldsymbol{\Omega}$ and terminal penalty matrix P by (5.9), (5.10), (5.11), (5.12), (5.13), and (5.14).

Step 3. Detect if formation state $X(t)$ enters the terminal region $\boldsymbol{\Omega}$ or not by (5.8). If it is true, then go to Step 8; else go to Step 4.

Step 4. Initialize particle swarm adopted with the last predictive control sequence $U(t-\delta)$ optimized by PSO, while particle swarm is initialed randomly at the first time.

Step 5. Evaluate the value of each particle by computing the cost function (5.15), and update the particle swarm and the global-best particle gbest according to (2.11).

Step 6. Detect if PSO precociously converge to local minima with (5.18). If it is true, then go to the next step; else go to Step 8.

Step 7. Use chaotic systems to generate a better solution to substitute random numbers for the PSO particles in next iteration and then go to Step 4.

Step 8. Detect the PSO terminate conditions (reaching the maximal generation or finding the idea optimum). If the terminate conditions are met, end the PSO algorithm and return the global-best particle *gbest* as the control sequence $U(t)$, or continue the computation.

Step 9. Apply the first part of the optimal control sequence to update formation state $X(t)$, and then go to Step 1.

Step 10. Use a linear state feedback $u = KX$ to control the nonlinear formation system to guarantee the stability of multiple UAV formation.

Step 11. Detect the formation stability conditions. If certain conditions are achieved, end the formation control method, or go to Step 2.

Figure 5.8 displays the flowchart of the chaotic PSO-based nonlinear dual-mode RHC formation control scheme for multiple UAV formation flight

5.2.4 Experiments

In this section, series experiments have been performed to investigate the performance of the proposed chaotic PSO-based nonlinear dual-mode RHC formation control scheme for multiple UAV formation flight. We use (5.1) to represent states of UAV model respectively. The multiple UAV group consists of 5 agents, with input constraints $[-5, 5]\text{m/s}^2$ for the acceleration u and $[-\pi/18, \pi/18]$ rad/s for the angular turn rate ω. To improve performance and avoid collisions, a safe distance between UAVs is defined, $d_{safe} = 3$. Collisions between UAVs are solved with the priority index strategy. Each UAV is tagged with a serial number.

The initial conditions of the nonlinear dual-mode formation controller are prediction horizon $T_p = 8\text{s}$, time step $\delta = 1\text{s}$ (the simulation time), weighting matrices $Q = \text{diag}(1,1,1,1)$, $R = \text{diag}(1,1)$, P =(0.0596 0 −0.0063 0;0 0.0596 0 −0.0063;−0.0063 0 0.0129 0;0 −0.0063 0 0.0129). The improved PSO parameter setting is the size of the particle swarm $p_s = 20$, inertia weight $w_{\max} = 1.2$, $w_{\min} = 0.1$, particle maximum velocity $vp_{\max} = 4$, $c_1 = 0.5$, $c_2 = 0.5$, and the maximum iteration $iter_{\max} = 200$.

In order to fully illustrate the efficiency of the proposed algorithm, we compare its performance with the standard GA under the same conditions. In both CPSO and GA, the population size is 20. The GA is real valued with random initialization and updates the population and search for the optimum with random techniques. Crossover and mutation probabilities are set as 0.8 and $1/n$, respectively, where n is the dimension of the problem.

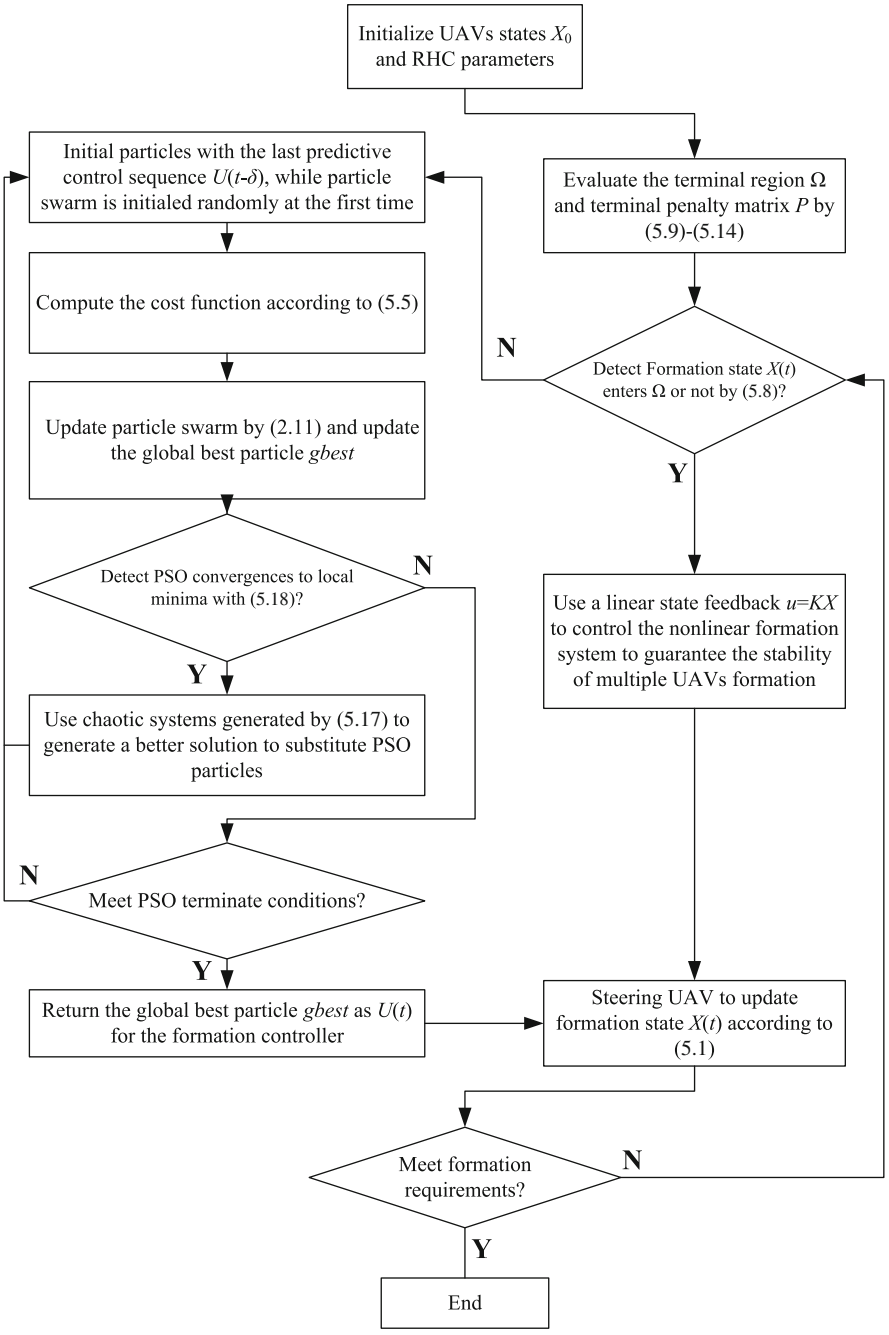

Fig. 5.8 Chaotic PSO-based RHC formation control scheme for multiple UAV formation flight (© [2002] IEEE. Reprinted, with permission, from Duan and Liu (2010))

5.2.4.1 Formation Control

Multiple UAV states are initialed as $\boldsymbol{x}_{VL}$ =(15,0,30,60), $\boldsymbol{x}_1$ =(15,0,5,65), $\boldsymbol{x}_2$=(15,0,5,75), $\boldsymbol{x}_3$ =(15,0,5,85), $\boldsymbol{x}_4$ =(15,0,5,45), $\boldsymbol{x}_5$ =(15,0,5,55), and the relative distances are $\boldsymbol{x}_{r1}$ =(0,0,0,0), $\boldsymbol{x}_{r2}$ =(0,0,−15,15), $\boldsymbol{x}_{r3}$ =(0,0,−30,30), $\boldsymbol{x}_{r4}$ =(0,0,−15,−15), $\boldsymbol{x}_{r5}$ =(0,0,−30,−30). The Virtual Leader is marked with "∘," while UAV is "Δ". The five UAVs reconfigure from a "|"initial shape to forming a "V" formation. Assume that the Virtual Leader speed is 15 m/s in the x-direction and its heading angle is 0 rad during the simulations. Figures 5.9 and 5.10 show the detailed results generated by the control sequence optimized by GA and CPSO, respectively.

The UAV group has to follow the Virtual Leader as seen in Fig. 5.9a, which shows the (x,y) positions of UAVs generated by using GA to optimize the control sequence. Note that the UAV group is traveling from left to right in the figure. The results are shown in Fig. 5.9, which illustrates that both the path tracking and formation maintenance tasks are not achieved. Figure 5.9b–e shows the multiple UAV convergence time. It is obvious that the 5th UAV cannot move to the initial relative position to follow the Virtual Leader, while other UAVs can converge to designated position. The same experiment is tested 5 times with similar results that the satisfactory tasks are not achieved.

In Fig. 5.10, UAVs follow the Virtual Leader with a constant velocity in x -direction and the desired separation between UAVs is 15 m in both the x - and y -directions. Under the control inputs optimized by CPSO, the multiple UAVs converge to the desired formation from the same initial configuration. Formation results are presented in Fig. 5.10a. The formations converge in 50s as seen in Fig. 5.10b. Compared with the results generated by the control sequence optimized by GA, CPSO performs better for its comprehensive ability to search and high precision, which demonstrates that CPSO is suitable for the dual-mode RHC controller.

5.2.4.2 Formation Control with an Obstacle

The second experiment illustrates the effectiveness of the proposed method in Sect. 4.2.3 for five UAVs performing obstacle avoidance. The parameters in the dual-mode RHC controller are chosen to be exactly the same as in the first experiment. The second experiment is initialed: $\boldsymbol{x}_{VL}$ =(15,0.7854,20,40), $\boldsymbol{x}_1$ =(5,0,−20,20), $\boldsymbol{x}_2$ =(5,0,20,20), $\boldsymbol{x}_3$ =(5,0,−40,20), $\boldsymbol{x}_4$ =(5,0,0,20), $\boldsymbol{x}_5$ =(5,0,−60,20), and the relative distances are $\boldsymbol{x}_{r1}$ =(0,0,0,0), $\boldsymbol{x}_{r2}$ =(0,0,−15,15), $\boldsymbol{x}_{r3}$ =(0,0,−30,30), $\boldsymbol{x}_{r4}$ =(0,0,−15,−15), $\boldsymbol{x}_{r5}$ =(0,0,−30,−30). And we change the Virtual Leader's heading angle from 0 to 0.7854 (π/4) and add a circular obstacle in the simulation environment. The obstacle center is located at (20, 40) and the radius is 12 m. Figure 5.11 shows the results generated by the control sequence optimized by GA, while Fig. 5.12 shows the results generated by the proposed algorithm.

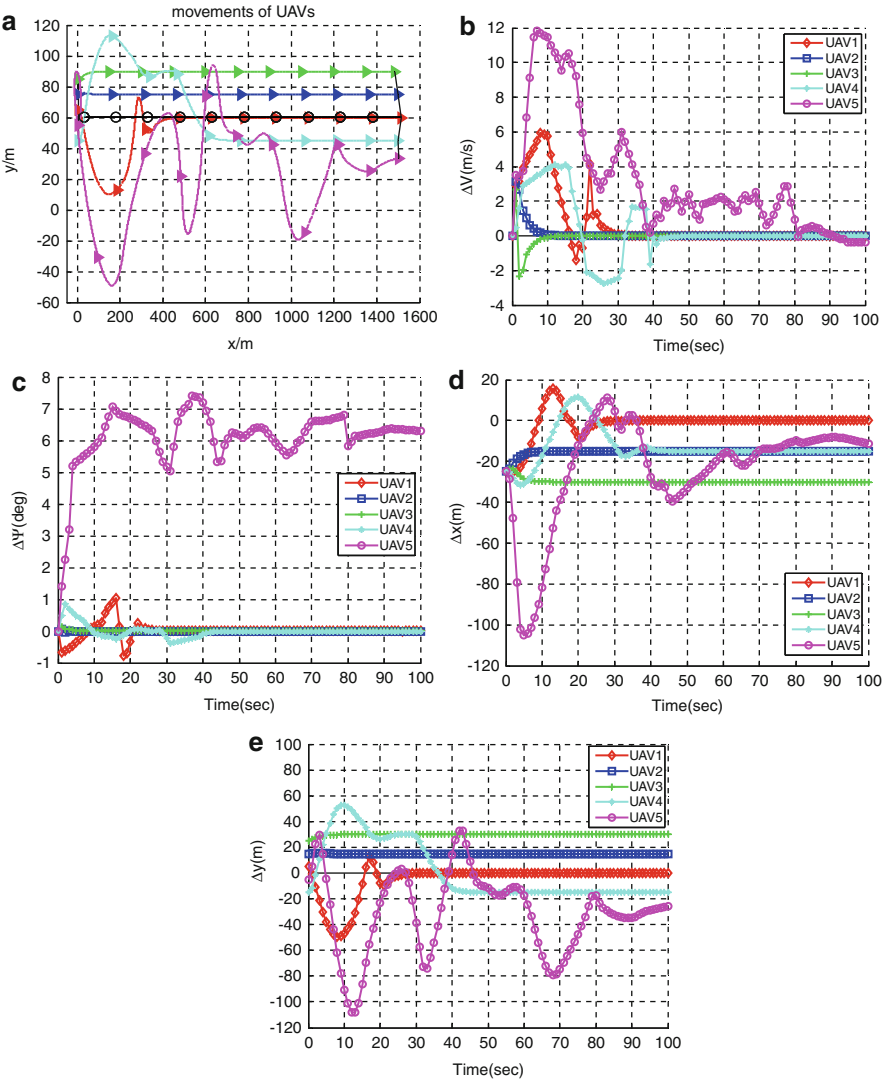

Fig. 5.9 The detailed results generated by the control sequence optimized by GA. (**a**) Five UAVs merge to a V-formation while following a Virtual Leader. (**b**) Relative velocities of 5 UAVs. (**c**) Relative heading angles. (**d**) Relative distances in the x-direction. (**e**) Relative distances in the y-direction (© [2002] IEEE. Reprinted, with permission, from Duan and Liu (2010))

The optimal obstacle avoidance trajectory with the dual-mode controller is generated assuming that UAVs can sense the circle obstacle. The trajectory of five UAVs after 20 time steps is presented in Figs. 5.11a and 5.12a. The results generated by control sequence optimized by GA as seen in Fig. 5.11b–e are far from satisfactory. Figure 5.12a shows the formation trajectory after 20 time steps.

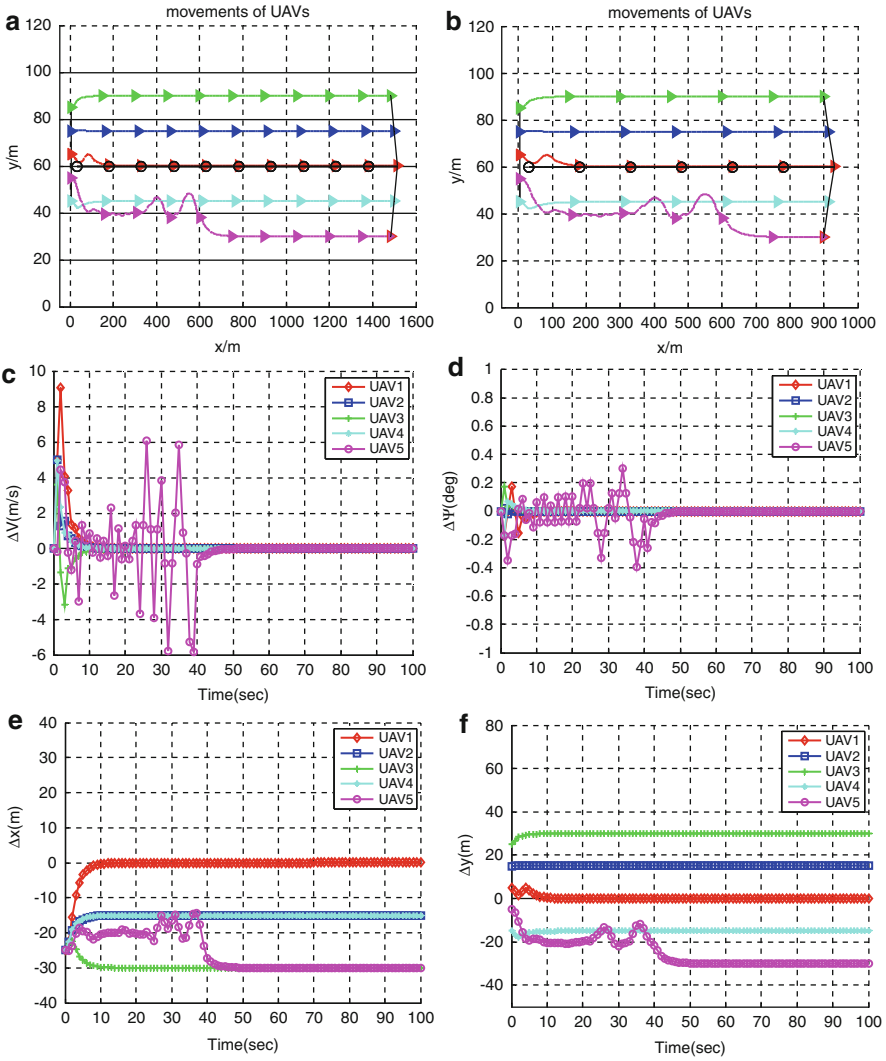

Fig. 5.10 The detailed results generated by the control sequence optimized by CPSO. (**a**) Formation trajectory under the same initial conditions. (**b**) Formation trajectory during the first sixty time steps. (**c**) Relative velocities of UAVs. (**d**) Relative heading angles. (**e**) Relative distances in the x -direction. (**f**) Relative distances in the y -direction (© [2002] IEEE. Reprinted, with permission, from Duan and Liu (2010))

The results are shown in Fig. 5.12c–d, which demonstrates that both the path tracking and formation maintenance tasks are successfully achieved. Figure 5.12c–e represents the multiple UAV convergence time. It is obvious that converge in 20s. It clearly shows the superiority of the proposed algorithm over GA.

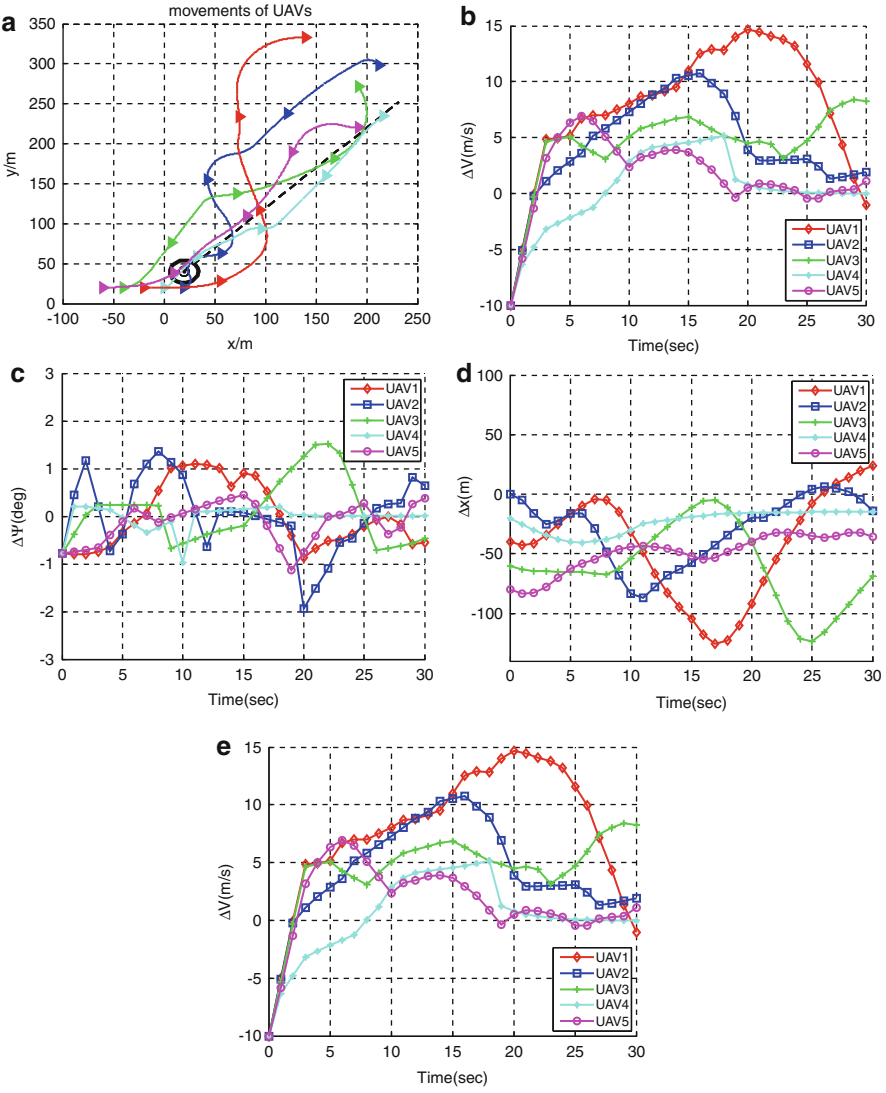

Fig. 5.11 The detailed results of GA for the second experiment. (**a**) Formation trajectory in a complicated environment with obstacle. (**b**) Relative velocities of UAVs. (**c**) Relative heading angles. (**d**) Relative distances in the x -direction. (**e**) Relative distances in the y -direction (© [2002] IEEE. Reprinted, with permission, from Duan and Liu (2010))

The simulation results obtained by applying the proposed dual-mode RHC algorithm show the UAVs are capable of flying in the desired formation. Simulations with different conditions are conducted to verify the feasibility and effectiveness of the proposed controller.

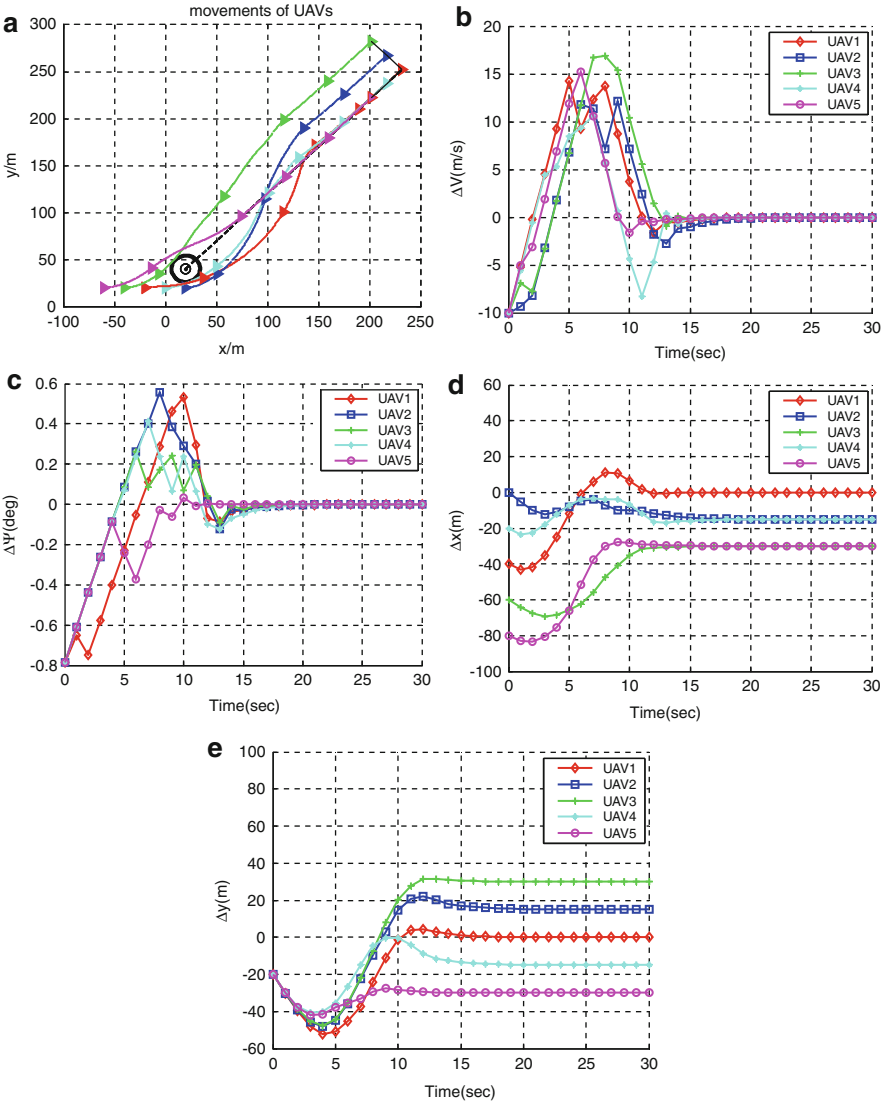

Fig. 5.12 The detailed results of CPSO for the second experiment. (**a**) Formation trajectory in a complicated environment with obstacle. (**b**) Relative velocities of UAVs. (**c**) Relative heading angles. (**d**) Relative distances in the x -direction. (**e**) Relative distances in the y -direction (© [2002] IEEE. Reprinted, with permission, from Duan and Liu (2010))

5.3 DE-Based RHC Controller for Multiple UAV Close Formation

5.3.1 Model of Multiple UAVs for Close Formation

In this section, a typical multiple UAV close formation model established by Proud et al. (1999) and Pachter et al. (2001) are adopted.

$$\begin{aligned}
\dot{x} &= -\frac{\overline{y}}{\tau_{\psi_W}} \cdot \psi_W - V_W + V_L \cos\psi_E + \frac{\overline{y}}{\tau_{\psi_W}} \cdot \psi_{W_C} + \overline{y}\frac{\overline{q}S}{mV}\left[\Delta C_{Y_{W_y}} \cdot y + \Delta C_{Y_{W_z}} \cdot z\right] \\
\dot{y} &= \frac{\overline{x}}{\tau_{\psi_W}} \cdot \psi_W + V_L \cdot \sin\psi_E - \frac{\overline{x}}{\tau_{\psi_W}} \cdot \psi_{W_C} - \overline{x}\frac{\overline{q}S}{mV}\left[\Delta C_{Y_{W_y}} \cdot y + \Delta C_{Y_{W_z}} \cdot z\right] \\
\dot{\psi}_W &= -\frac{1}{\tau_{\psi_W}} \cdot \psi_W + \frac{1}{\tau_{\psi_W}} \cdot \psi_{W_C} + \frac{\overline{q}S}{mV}\left[\Delta C_{Y_{W_y}} \cdot y + \Delta C_{Y_{W_z}} \cdot z\right] \\
\dot{V}_W &= -\frac{1}{\tau_{V_W}} \cdot V_W + \frac{1}{\tau_{V_W}} \cdot V_{W_C} + \frac{\overline{q}S}{m} \cdot \Delta C_{D_{W_z}} \cdot z \\
\dot{z} &= \zeta \\
\dot{\zeta} &= -\left(\frac{1}{\tau_a} + \frac{1}{\tau_b}\right) \cdot \zeta - \frac{1}{\tau_a \tau_b} z + \frac{1}{\tau_a \tau_b} h_{W_C} - \frac{1}{\tau_a \tau_b} h_{L_C} + \frac{\overline{q}S}{m} \cdot \Delta C_{L_{W_y}} \cdot y
\end{aligned} \tag{5.20}$$

The optimal separation between the Wingman and Leader UAV can be described with $\overline{x} = 2b, \overline{y} = \pi b/4, \overline{z} = 0$, where b is the wingspan of the Leader. The close formation model is established based on the aerodynamic forces on the Wing UAV near the optimal relative position, with a rotating reference frame affixed to the Wingman's instantaneous position and aligned with the Wingman's velocity vector used.

In the close formation model shown in (5.20), (x,y,ψ_W,V_W,z,ζ) are the state vectors, where x, y, and z denote the longitudinal, lateral, and vertical separation between the Leader and Wingman, respectively. ψ_W and V_W denote the heading angle and velocity of the Wingman, respectively. ($\psi_{W_C}, V_{W_C}, h_{W_C}$) are the control inputs to Wingman's heading hold, mach hold, and altitude hold autopilot channels, respectively. The Leader's maneuvers are regarded as a disturbance, which can be expressed with (ψ_L, V_L, h_{L_C}).

5.3.2 Description of RHC-Based Multiple UAV Close Formation

When multiple UAVs fly in a close formation, the Wingman must maintain itself at the optimal separation which is measured with respect to the Leader's position. Thus, the cost function (or objective function) of multiple UAV close formation flight can be described with a quadratic form (Zhang and Duan 2012):

$$\begin{aligned} \min J &= \int_0^T \left(\left(\boldsymbol{X}_{ref} - \boldsymbol{x}(t)\right)^T \cdot \boldsymbol{Q} \cdot \left(\boldsymbol{X}_{ref} - \boldsymbol{x}(t)\right) dt \\ s.t.\ \boldsymbol{x}(t) &= \int_0^t \boldsymbol{f}\left(\boldsymbol{x}(0), \boldsymbol{u}(\tau), \boldsymbol{d}(\tau)\right) d\tau \\ \boldsymbol{U}_{\min} &\le \boldsymbol{u}(t) \le \boldsymbol{U}_{\max} \end{aligned} \tag{5.21}$$

where $\boldsymbol{x}(t) = [x,y,z,V_W,\psi_W]^T$ denotes the formation state, and the control inputs of Wingman's autopilot is represented by $\boldsymbol{u}(t) = [V_{W_C}, \psi_{W_C}, h_{W_C}]^T$. $\boldsymbol{X}_{ref} = [x_C,y_C,z_C,V_L,\psi_L]^T$ represents the reference state of the close formation system, and x_C, y_C, z_C determines the formation geometry. In the close formation model adopted in our work, Leader's flight states' change can break the formation's stability. In this way, Leader's maneuver can be regarded as the disturbance to the flight formation, described as $\boldsymbol{d}(t)$. $\boldsymbol{Q} = diag\{q_1, \cdots, q_5\}$ is a positive-definite matrix.

RHC divides the global control problem into some local optimization problems at receding time horizons. These local optimization problems have the same optimization objectives with the global control problem. In the kth sampling instant, the dynamic of the close formation can be written as:

$$\begin{aligned} \boldsymbol{x}(k+1) &= \boldsymbol{x}(k) + \int_{kT}^{(k+1)T} \boldsymbol{f}\left(\boldsymbol{x}(k), \boldsymbol{u}(k)\right) dt = \boldsymbol{f}_d\left(\boldsymbol{x}(k), \boldsymbol{u}(k), \boldsymbol{d}(k)\right) \\ \boldsymbol{x}(0) &= \boldsymbol{x}_0 \end{aligned} \tag{5.22}$$

The control inputs of the Wingman are subject to the following constraints:

$$U = \{\boldsymbol{u}(k) \,||\, \boldsymbol{U}_{\min} \le \boldsymbol{u}(k) \le \boldsymbol{U}_{\max}\} \tag{5.23}$$

where $\boldsymbol{x}(k) \in \mathbf{R}^5$ represents the formation state at the kth sampling time, and the control action, keeping constant until next predictive horizon, is represented by $\boldsymbol{u}(k) \in \boldsymbol{R}^3$. $\boldsymbol{d}(k) \in \boldsymbol{R}^3$ describes the Leader's state. T denotes the span of one time horizon, or sampling interval.

Assumption 1 *The multiple UAV close formation system given in* (5.20) *is controllable and stabilizable.*

Taking into account various practical constraints, such as the UAV's physical performance and the flight mission requirements, Wingman's control action $\boldsymbol{u}$ is

always available with the Leader's state $\boldsymbol{d}$, which can stably maintain the formation state as the reference $\boldsymbol{X}_{ref}$, i.e., $\forall\, \boldsymbol{d}$, $\exists\, \boldsymbol{u} \in U$, subject to $\boldsymbol{X}_{ref} = \boldsymbol{f}_d(\boldsymbol{X}_{ref}, \boldsymbol{u}, \boldsymbol{d})$.

At time k, RHC controller computes predictive control sequences of current and future p predictive time horizons according to the formation's current state, which can be represented as $\boldsymbol{u}(k|k)$, $\boldsymbol{u}(k+1|k)$, $\cdots$, $\boldsymbol{u}(k+p-1|k)$. Suppose that Leader's state will not change in the following p time horizons, namely, $\boldsymbol{d}(k+i) = \boldsymbol{d}(k)$. Then the states of the formation in these time horizons $\boldsymbol{x}(k+1|k)$, $\boldsymbol{x}(k+2|k)$, $\cdots$, $\boldsymbol{x}(k+p|k)$ can be obtained. The next p time horizons are named as predictive time horizon.

Denote the quadratic cost by the following fitness function at the kth time:

$$\begin{aligned}
&\min J(k) = \sum_{i=1}^{p} \left[\left(\boldsymbol{X}_{ref} - \boldsymbol{x}\left(k+i\middle|k\right)\right)^T \cdot \boldsymbol{Q} \cdot \left(\boldsymbol{X}_{ref} - \boldsymbol{x}\left(k+i\middle|k\right)\right)\right. \\
&s.t.\ \boldsymbol{x}\left(k+1\middle|k\right) = \boldsymbol{f}_d\left(\boldsymbol{x}(k|k), \boldsymbol{u}(k|k), \boldsymbol{d}(k)\right) \\
&\boldsymbol{x}\left(k+j+1\middle|k\right) = \boldsymbol{f}_d\left(\boldsymbol{x}(k+j|k), \boldsymbol{u}(k+j|k), \boldsymbol{d}(k)\right) \\
&\boldsymbol{U}_{\min} \le \boldsymbol{u}\left(k+j\middle|k\right) \le \boldsymbol{U}_{\max}
\end{aligned} \tag{5.24}$$

Minimize fitness function (5.24); the optimal solution to the local optimization problem at time k can be obtained, which is represented by $\boldsymbol{u}^*(k+j-1|k)$, $j = 1, \cdots, p$. Apply the preceding m control actions $\boldsymbol{u}^*(k|k)$, $\boldsymbol{u}^*(k+1|k)$, $\cdots$, $\boldsymbol{u}^*(k+m-1|k))$, $(0 \le m \le p)$ to the formation-hold control system residing on Wingman successively in current and following $m-1$ time horizons. Subsequently, at time $k+m$, repeat sampling, predicting, optimization, and implementing. By using this receding optimization technique, multiple UAV close formation state can approximate to the reference value finally. Dunbar and Murray (2006) theoretically demonstrated the stability of distributed MPC with a sufficiently fast update period. This process can be described as Fig. 5.13.

RHC treats the global control problem as a series of online local optimization problems. However, multiple UAV formation reconfiguration problem is actually constrained nonlinear optimization problems and is very difficult to be solved by using the traditional approaches. However, numerous population-based optimization approaches can provide good solutions to these complicated problems. DE algorithm is utilized to optimize the fitness function, and the predictive control law can be optimized directly.

5.3.3 DE-Based RHC Controller Design for Close Formation

5.3.3.1 Controller Design

The formation flight controller is equipped on the Wing UAV. It is an outer-loop controller that receives measurements of separation between the Leader and

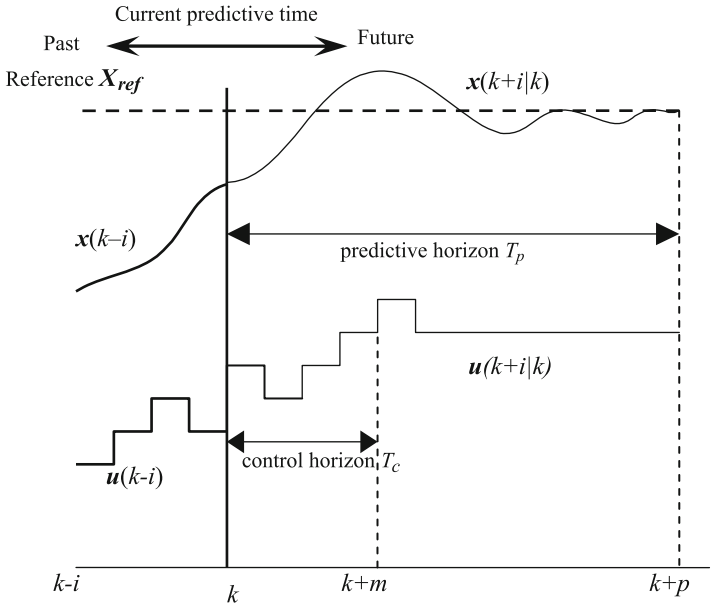

Fig. 5.13 Basic ideas of RHC (Reprinted from Zhang et al. (2010), with kind permission from Springer Science+Business Media)

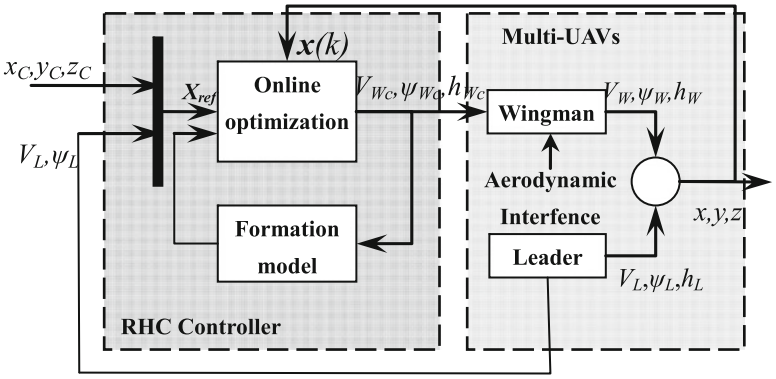

Fig. 5.14 Frame of multiple UAV close formation controller-based RHC (Reprinted from Zhang et al. (2010), with kind permission from Springer Science+Business Media)

Wingman and drives the control signals of the Wingman's three channels: mach hold, heading hold, and altitude hold autopilot. The block diagram of DE-based RHC controller for multiple UAV close formation is shown in Fig. 5.14 (Zhang and Duan 2012):

Models of each single UAV are low-order models: the heading hold and the mach hold autopilot are first order, and the altitude hold autopilot is second order.

$$\begin{aligned}
\dot{\psi}_W &= -\frac{1}{\tau_{\psi_W}} \cdot \psi_W + \frac{1}{\tau_{\psi_W}} \cdot \psi_{W_C} \\
\dot{V}_W &= -\frac{1}{\tau_{V_W}} \cdot V_W + \frac{1}{\tau_{V_W}} \cdot V_{W_C} \\
\ddot{h}_W &= -\left(\frac{1}{\tau_a} + \frac{1}{\tau_b}\right) \cdot \dot{h}_W - \frac{1}{\tau_a \cdot \tau_b} \cdot h_W + \frac{1}{\tau_a \cdot \tau_b} \cdot h_{W_C}
\end{aligned} \tag{5.25}$$

In the online optimization process, set (5.24) as the fitness function of DE (Price and Storn 1997), and set predictive control sequence $\boldsymbol{u}(k+i-1|k)$, $i=1,\cdots,p$ as the individual vector, which is just the objective of DE optimization operations. Here, the length of the predictive horizon is p, and thus DE's search region is a $D=3p$ -dimensional space. At time k, the jth individual of DE algorithm is represented by $\boldsymbol{x}_j$ $=[V_{Wc}{}^j(k|k),\ \psi_{Wc}{}^j(k|k),\ h_{Wc}{}^j(k|k),\ \ldots,\ V_{Wc}{}^j(k+p-1|k),\ \psi_{Wc}{}^j(k+p-1|k), h_{Wc}{}^j(k+p-1|k)]$. Apply DE's evolutionary operators to $\boldsymbol{x}_j$ until the terminal criterion is satisfied, and then choose the individual with the smallest fitness function value as the optimal control sequence. After that, implement the preceding $3\cdot m$ control actions to the Wing UAV's autopilot at each time horizon respectively.

With the purpose of improving the online searching efficiency and making full use of all aspects of information, for the solution $\boldsymbol{x}_j^{\kappa}$ $=[V_{Wc}{}^j(k+\kappa|k),\ \psi_{Wc}{}^j(k+\kappa|k),\ h_{Wc}{}^j(k+\kappa|k)]$, $\kappa=0,\cdots,p-1$ at time $k+\kappa$ with respect to the individual $\boldsymbol{x}_j$ of DE population, one feasible method used is to assign their initial value in the following three steps: (i) Set them as Leader's current state $[V_L(k+\kappa), \psi_L(k+\kappa), h_L(k+\kappa)]$. (ii) Set them as former one time horizon's control action $[V_{Wc}{}^j(k+\kappa-1|k),\ \psi_{Wc}{}^j(k+\kappa-1|k),\ h_{Wc}{}^j(k+\kappa-1|k)]$. (iii) Assign their values randomly.

In order to reduce the computing complexity, we adopted the one step predictive control, i.e., $m=p=1$.

When multiple UAVs fly in a close formation, at the kth time horizon, the DE-based RHC controller implements the process online in the following steps:

Step 1: Input the formation's current state $\boldsymbol{x}(k)=[x,y,z,V_W,\psi_W]^T$ as well as Leader's state $[V_L(k), \psi_L(k), h_L(k)]$, compare them with the reference state $\boldsymbol{X}_{ref}(k)$, and then optimize the predictive control law.

Step 2: Initialize the DE population (each individual of the DE's population is a reference solution to $\boldsymbol{u}(k|k)$), and set their initial values as follows:

$$\boldsymbol{x}_j = \begin{cases} \left[V_L(k), \psi_L(k), h_L(k)\right], & j=1 \\ \left[V_{Wc}(k-1), \psi_{Wc}(k-1), h_{Wc}(k-1)\right], & j=2 \\ rand\cdot(\boldsymbol{U}_{\max}-\boldsymbol{U}_{\min})+\boldsymbol{U}_{\min}, & else \end{cases}$$

where $j=1,\cdots D$.

Step 3: Compute the fitness function value $f(\boldsymbol{x}_j)$.

Step 4: Apply DE's mutation and recombination operators to $\boldsymbol{x}_j$, and generate the trial vector $\boldsymbol{u}_j$, and then compute its fitness function value $f(\boldsymbol{u}_j)$.

Step 5: Compare $f(\boldsymbol{u}_j)$ and $f(\boldsymbol{x}_j)$, implement DE's selection operator, and then move the individual with the lowest fitness value to the next generation. Go to Step 3 until stopping criterion is satisfied.

Step 5: The best individual of DE population is just the optimal control input $\boldsymbol{u}^*(k|k)$; output and apply it to each autopilot.

Step 7: Go to **Step 1** and move forward into the $(k+1)$th time horizon.

5.3.3.2 Stability Analysis

Let $\boldsymbol{u}^*(k|k)$ be the optimal predictive control sequence at time k. If this control sequence continues to work until time $k+2$, the multiple UAV close formation system state at time $k+2$ can be obtained by

$$\boldsymbol{x}(k+2) = \int_{kT}^{(k+2)T} \boldsymbol{f}\left(\boldsymbol{x}(\tau), \boldsymbol{u}*\left(k\middle|k\right), \boldsymbol{d}(k)\right) d\tau \tag{5.26}$$

According to the further analysis, the fitness function $J(k)$ of $\boldsymbol{u}(k|k)$ depends on the state $\boldsymbol{x}(k+1)$ at time $k+1$. Using $\boldsymbol{u}^*(k|k)$ yielded by the DE optimization, the multiple UAV formation state at time k+1 will be the optimal:

$$\boldsymbol{x}*(k+1) = \int_{kT}^{(k+1)T} \boldsymbol{f}\left(\boldsymbol{x}(\tau), \boldsymbol{u}*\left(k\middle|k\right), \boldsymbol{d}(k)\right) d\tau \tag{5.27}$$

Continue using $\boldsymbol{u}^*(k|k)$ at the next time horizon, i.e., let $\boldsymbol{u}(k+1|k+1)=\boldsymbol{u}^*(k|k)$. However, this cannot guarantee that the fitness function value $J(k+1)$ is the optimal. Therefore, the system state at time $k+2$:

$$\boldsymbol{x}(k+2) = \int_{(k+1)T}^{(k+2)T} \boldsymbol{f}\left(\boldsymbol{x}(\tau), \boldsymbol{u}*\left(k\middle|k\right), \boldsymbol{d}(k)\right) d\tau \tag{5.28}$$

is not optimal.

At time $k+1$, optimize $\boldsymbol{u}(k+1|k+1)$ by using DE algorithm. Since the initial population has contained last time's control input $\boldsymbol{u}^*(k|k)$, together with Lemma 2, the system state at time $k+2$

$$\boldsymbol{x}^*(k+2) = \int_{(k+1)T}^{(k+2)T} \boldsymbol{f}\left(\boldsymbol{x}(\tau), \boldsymbol{u}^*\left(k+1\middle|k+1\right), \boldsymbol{d}(k+1)\right) d\tau \tag{5.29}$$

is superior to $\boldsymbol{x}(k+2)$ determined by (5.28) and $J^*(k+1) \le J(k+1)$.

In which, the control sequence $\boldsymbol{u}^*(k|k), \boldsymbol{u}^*(k+1|k+1), \ldots, \boldsymbol{u}^*(k+N|k+N)$ driving the system's fitness function value is always superior to that at the last

time horizon. Given an appropriate control step, the system's fitness function will converge to the stable value. Thus, the multiple UAV close formation system can be stabilized at the reference state.

5.3.4 Experiments

In order to investigate the feasibility and effectiveness of our proposed DE-based RHC approach to multiple UAV close formation control, two experiments were conducted. The proposed approach was coded in MATLAB language and implemented on PC-compatible with 2 GB of RAM under the Microsoft Windows Vista.

In all experiments, the initial separations between Leader and Wingman were set with $x_C = 60$ft, $y_C = 23.6$ft, $z_C = 0$ft. The model parameters in (5.20) were from Proud et al. (1999). Given Leader's heading angle and velocity were $\psi_L = 0^o$ and $V_L = 200$ft/s at the beginning of the experiments, while at time $t = 5$s, the Leader's flight states turned to $\psi_L = 20^o$ and $V_L = 250$ft/s. The experiments were performed with 30 s, and the following results show the response curves of the longitudinal and lateral separation, Wing UAV's heading and velocity, as well as the final fitness value at each prediction horizon.

The parameters of DE-based RHC controller are set as follows: $F = 1.4$, $CR = 0.5$, $NP = 10$, $NC = 20$, $m = p = 1$, $Q =$ diag[100,100,1,1].

1. Consider the aerodynamic interference introduced by Leader, and set the sampling interval at $Ts = 0.1$s. The time response is shown as Fig. 5.15.
2. Change the sampling time interval as $Ts = 0.01$s.The simulation results are shown in Fig. 5.16.

The comparative results in Figs. 5.15 and 5.16 show that the shorter the sampling period, the more stable the time response for the multiple UAV close formation system. It is obvious that better performance can be obtained by shortening the prediction horizon.

5.4 DE-Based RHC Controller for Multiple UAV Formation Reconfiguration

5.4.1 Model of Multiple UAVs for Formation Configuration

We consider a group of N UAVs are flying at the same altitude without sideslip, and they turn through the coordinated turn. For each UAV in the flight formation, its state variable is set as $\boldsymbol{x}_i = (v_i, \psi_i, x_i, y_i)^T$, $i = 1, \cdots, N$, and the dynamic of the single UAV can be written as

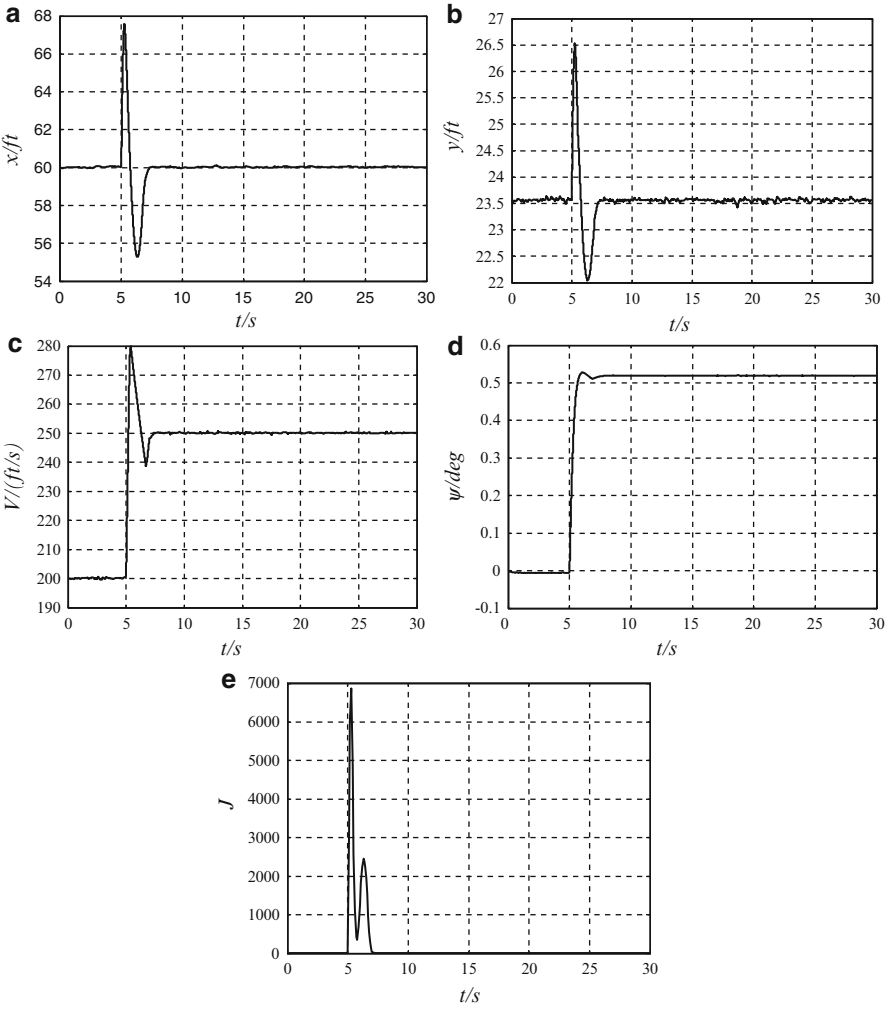

Fig. 5.15 Time response of multiple UAV close formation system ($T_s = 0.1$s). (**a**) Longitudinal separation x. (**b**) Lateral separation y. (**c**) Wingman's velocity V_W. (**d**) Wingman's heading ψ_W. (**e**) Optimal fitness value $J^*(k)$ (Reprinted from Zhang et al. (2010), with kind permission from Springer Science+Business Media)

$$\begin{aligned}
\dot{v} &= (T - D)/W \\
\dot{\psi} &= g \cdot \sin\varphi / v \\
\dot{x} &= v \cdot \cos\psi \\
\dot{y} &= v \cdot \sin\psi
\end{aligned} \tag{5.30}$$

where v is the horizontal flying velocity of each UAV in the flight formation, ψ denotes the heading angle, and the UAV's horizontal location is represented by

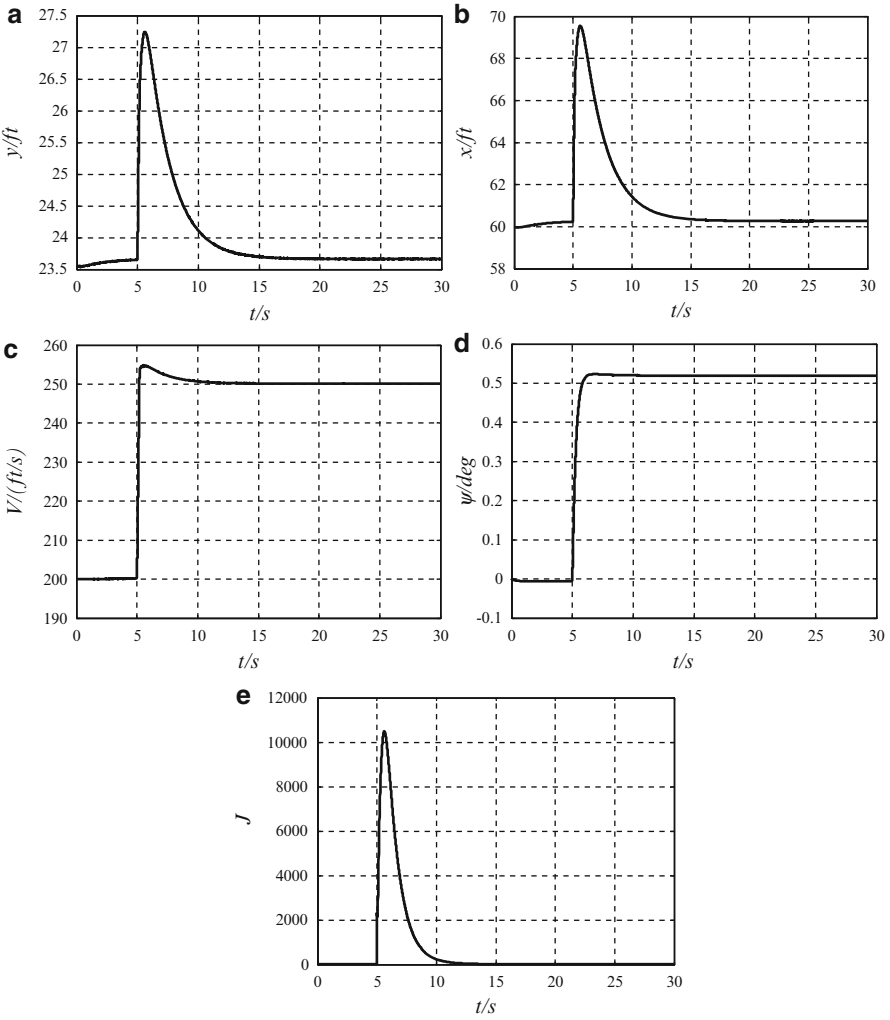

Fig. 5.16 Time response of multiple UAV close formation system ($Ts = 0.01$s). (**a**) Longitudinal separation x. (**b**) Lateral separation y. (**c**) Wingman's velocity V_W. (**d**) Wingman's heading ψ_W. (**e**) Optimal fitness value $J^*(k)$ (Reprinted from Zhang et al. (2010), with kind permission from Springer Science+Business Media)

(x,y) in the earth-surface inertial reference frame. The control inputs of each UAV's autopilot are represented by $\boldsymbol{u} = (T,\varphi)^T$, which contain the thrust T and the roll angle φ. D represents the aerodynamic drag, which is simply regarded as a constant. The weight of each UAV is W, and gravity acceleration $g = 9.8m/s^2$. Thus, dynamics of the ith UAV can be described as

$$\dot{x}_i(t) = f\left(x_i(t), u_i(t)\right), i = 1, \cdots, N \tag{5.31}$$

Set one UAV in the formation as the Leader, which is treated as the reference point, and its state vector is represented by $\boldsymbol{x}_L$. Relative to the Leader UAV, $(\boldsymbol{x}_i - \boldsymbol{x}_L)$ denotes the relative state of the ith UAV. Assume the initial time of the reconfiguration process is $t_0 = 0$, and the terminal time is $t = T$. The process of the formation reconfiguration is regarded as a control optimization problem, and so, the goal is to find the continuous control action $\boldsymbol{U} = (\boldsymbol{u}_1, \cdots, \boldsymbol{u}_N)$ that minimize a cost function that enables the terminal positions of every UAV to reach their desired value. Set the cost function as the quadratic form, which is described in the following equation:

$$\begin{aligned} \min J(U) = & \sum_{i=1}^{N} \left(x_{ref,i} - \left(x_i \left(T \middle| u_i \right) - \boldsymbol{x}_L \left(T \middle| u_L \right) \right) \right)^T \\ & Q \left(x_{ref,i} - \left(x_i \left(T \middle| u_i \right) - x_L \left(T \middle| u_L \right) \right) \right) \\ s.t.\ \boldsymbol{x}_i & \left(t \middle| \boldsymbol{u}_i \right) = \boldsymbol{x}_i(0) + \int_0^t f\left(\boldsymbol{x}_i(\tau), \boldsymbol{u}_i(\tau) \right) d\tau \\ & \boldsymbol{U}_{\min} \leq \boldsymbol{U} \leq \boldsymbol{U}_{\max} \end{aligned} \tag{5.32}$$

where $\boldsymbol{X}_{ref} = [\boldsymbol{x}_{ref,1}, \cdots, \boldsymbol{x}_{ref,N}]$ represents the terminal reference state of the multiple UAV system, which defines the terminal shape of the multiple UAV formation. $\boldsymbol{x}_i(T|\boldsymbol{u}_i)$ denotes the ith UAV's terminal state driving by the control input $\boldsymbol{u}_i$. For each UAV, given the initial state $\boldsymbol{x}_i(0)$, its state $\boldsymbol{x}_i(t)$ at any time t can be uniquely determined by $\boldsymbol{u}_i$. The control inputs are constrained by the performance of UAVs. $\boldsymbol{Q} = \text{diag}\{q_1, q_2, q_3, q_4\}$ is a positive-definite matrix.

Denote the distance between any two UAV as $d_{i,j}(t)$, $i, j = 1, \cdots, N$, which is computed as

$$d_{i,j}(t) = \sqrt{\left(x_i(t) - x_j(t) \right)^2 - \left(y_i(t) - y_j(t) \right)^2}$$

In order to avoid collision between two UAVs, $d_{i,j}(t)$ must be greater than the safe anti-collision distance D_{safe}, that is,

$$d_{i,j}(t) \geq D_{safe}, \forall t \in [0, T], \forall_{i \neq j} i, j \in \{1, \cdots, N\} \tag{5.33}$$

In order to ensure the real-time communication to achieve the information sharing, $d_{i,j}(t)$ must be less than the communication distance D_{com}, that is,

$$d_{i,j}(t) \leq D_{com}, \forall t \in [0, T], \forall_{i \neq j} i, j \in \{1, \cdots, N\} \tag{5.34}$$

Comprehensively consider the distance-restrictive conditions as shown in (5.33) and (5.34); the extended cost function can be rewritten as

$$\min J_{extend}(\boldsymbol{U}) = J(\boldsymbol{U}) + \omega \cdot \int_0^T \sum_{i \neq j} \left[\max\left(0, D_{safe} - d_{i,j}(t)\right) + \max\left(0, d_{i,j}(t) - D_{com}\right)\right] dt \tag{5.35}$$

where ω denotes the distance punishment constant coefficient, and it should be great enough so that the distance restricts of multiple UAV formation can be satisfied and $\omega = 10^{10}$.

5.4.2 Description of RHC-Based Multiple UAV Formation Reconfiguration

RHC divides the global control problem into some local optimization problems at receding time horizons. These local optimization problems have the same optimization objectives as the global control problem. In the kth sampling instant, the dynamic of the ith UAV of multiple UAV formation can be written as

$$\boldsymbol{x_i}(k+1) = \boldsymbol{x}_i(k) + \int_{kT}^{(k+1)T} f(\boldsymbol{x}_i(k), \boldsymbol{u}_i(k)) dt \tag{5.36}$$

The control inputs subject to the following constraints:

$$U = \{\boldsymbol{u_i}(k) \,||\, \boldsymbol{u}_{\min} \leq \boldsymbol{u_i}(k) \leq \boldsymbol{u}_{\max}\} \tag{5.37}$$

where $\boldsymbol{x_i}(k) = [v_i(k), \psi_i(k), x_i(k), y_i(k)] \in \boldsymbol{R}^4$ represents the ith UAV's state at the kth sampling time, and the control input of the ith UAV, keeping constant until the next predictive horizon, is represented by $\boldsymbol{u}_i(k) = [T_i(k), \varphi_i(k)] \in \boldsymbol{R}^3$. T denotes the span of one time horizon or sampling interval.

At time k, RHC controller computes predicted control sequences of the current and future p predicted time horizons for each UAV according to multiple UAVs' current state and the constraint, and these control inputs can be represented by $\boldsymbol{u}_i(k|k)$, $\boldsymbol{u}_i(k+1|k)$, $\cdots$, $\boldsymbol{u}_i(k+p-1|k)$. Then, the predictive states of each UAV in the next p time horizons can be obtained, which are represented by $\boldsymbol{x}_i(k+1|k)$, $\boldsymbol{x}_i(k+2|k)$, $\cdots$, $\boldsymbol{x}_i(k+p|k)$. The next p time horizons are called predictive time horizon.

Denote the quadratic cost by the following fitness function at the kth time:

$$\begin{aligned}
\min J(k) = \sum_{j=1}^{p}\sum_{i=1}^{N}\left(x_{ref,i} - \left(\boldsymbol{x}_i\left(k+j\middle|k\right) - x_L\left(k+j\middle|k\right)\right)\right)^T Q \\
\left(x_{ref,i} - \left(x_i\left(k+j\middle|k\right) - x_L\left(k+j\,|\,k\right)\right)\right) \\
s.t.\ \boldsymbol{x}_i\left(k+1\middle|k\right) = \boldsymbol{x}_i(k) + \int_0^T f\left(\boldsymbol{x}_i(k), \boldsymbol{u}_i\left(k\middle|k\right)\right)dt \\
\boldsymbol{x}_i\left(k+j+1\middle|k\right) = \boldsymbol{x}_i\left(k+j\,|\,k\right) + \int_0^T f\left(\boldsymbol{x}_i\left(k+j\middle|k\right), \boldsymbol{u}_i\left(k+j\middle|k\right)\right)dt \\
\boldsymbol{u}_{\min} \le \boldsymbol{u}_i\left(k+j\middle|k\right) \le \boldsymbol{u}_{\max}
\end{aligned} \tag{5.38}$$

Minimize fitness function (5.38); the optimal control solution to the local optimization problem at time k can be obtained, which is represented by $\boldsymbol{u}_i{}^*(k+j-1|k)$, $j=1,\cdots,p$. Apply the preceding m control actions $\boldsymbol{u}^*(k|k)$, $\boldsymbol{u}^*(k+1|k)$, $\cdots$, $\boldsymbol{u}^*(k+m-1|k))$, $(0 \le m \le p)$ to each UAV's autopilot successively in current and following $m-1$ time horizons. Subsequently, at time $k+m$, repeat sampling, predicting, optimization, and implementing. By using this receding technique, multiple UAV formation's state can approximate to the reference value finally.

RHC treats the global control problem as a series of online local optimization problems. However, multiple UAV formation reconfiguration problem is actually constrained nonlinear problems and is difficult to be solved by using the traditional approaches. The method to compute the control law is a key technique to RHC. Numerous population-based optimization approaches provide good solutions to these complicated problems. DE algorithm is utilized to optimize the fitness function, and the RHC control law can be worked out directly.

5.4.3 DE-Based RHC Controller Design for Formation Reconfiguration

DE algorithm is utilized to solve the predictive control law directly. The block diagram of DE-based RHC controller for multiple UAV formation reconfiguration process is shown in Fig. 5.17 (Zhang et al. 2010).

In the online reconfiguration process, set (5.37) as the fitness function of DE, and set predicted control sequence $\boldsymbol{u}(k+i-1|k)$, $i=1,\cdots,p$ as the individual vector, which is just the objective of DE operators. For the flight formation of N UAVs, the length of the predicted horizon is p and the control input has two actions: thrust and roll angle, so the DE's search region is a $D=2\cdot N\cdot p$ -dimensional space. At time k, the ath individual of DE is represented by $x_a = [T_1(k|k), \varphi_1(k|k), \ldots, T_i(k|k), \varphi_i(k|k), \ldots, T_N(k|k), \varphi_N(k|k), \ldots,$

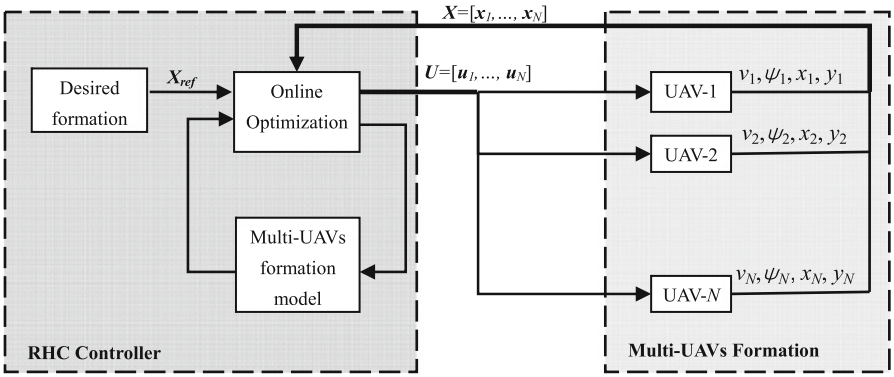

Fig. 5.17 Block diagram of formation reconfiguration (Reprinted from Zhang and Duan (2012), with kind permission from SAGE Publications)

$T_i(k+j-1|k), \varphi_i(k+j-1|k), \ldots]$, where $a = 1, \cdots NP$, $i = 1, \cdots N$, $j = 1, \cdots p$. Apply DE's evolutionary operators to x_a until the terminal criterion is satisfied, and then choose the individual with the lowest fitness function value as the optimal control sequence. After that, implement the preceding $2 \cdot N \cdot m$ control actions to corresponding UAV at each time horizon respectively.

In order to reduce the computing complexity, we adopt the one step predicted control, i.e., $m = p = 1$.

When multiple UAV is flying in a formation, at the kth time horizon, the flight formation receives the command that a new formation is inevitable, and thus, the DE-based RHC controller implements the process online in the following steps:

Step 1: Set the parameters of RHC and DE.

Step 2: Input each UAV's current state $\boldsymbol{X}(k) = [\boldsymbol{x}_1, \cdots, \boldsymbol{x}_N]$ as well as the desired formation shape and then carry on the optimization process.

Step 3: Initialize the DE population (each individual of the population is a candidate solution to $\boldsymbol{U}(k|k)$). In order to improve the online searching efficiency and make full use of all aspects of information, half individuals of the population are chosen randomly, and others are set as the control actions $\boldsymbol{U}(k-1)$ at the former one time horizon.

Step 4: Compute the fitness function value $f(x_a)$.

Step 5: Apply DE's mutation and recombination operators to x_a and generate trial vector u_a, and then compute its fitness function value $f(u_a)$.

Step 6: Compare $f(u_a)$ and $f(x_a)$, implement DE's selection operator, and then preserve the individual with the lower fitness value in the next generation. Go to Step 4 until the stopping criterion is satisfied.

Step 7: The best individual of DE population is just the optimal control sequence $\boldsymbol{U}^*(k|k)$; output and apply them to each UAV respectively.

Step 8: Go to Step 2 and move forward into next $(k+1)$th time horizon.

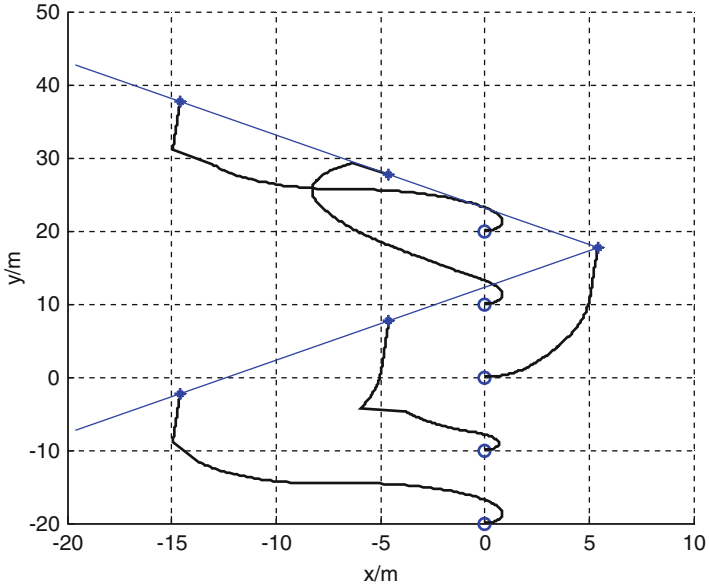

Fig. 5.18 Reconfiguration trajectory of multiple UAVs; "o" is the initial position, and "•" is the terminal position (Reprinted from Zhang and Duan (2012), with kind permission from SAGE Publications)

5.4.4 Experiments

In order to investigate the feasibility and effectiveness of our proposed DE-based RHC approach to the problem of the multiple UAV formation reconfiguration control, a series of experiments were conducted under the complicated combating environment. The proposed approach was coded in MATLAB language and implemented on PC-compatible with 2 GB of RAM under the Microsoft Windows Vista.

In all experiments, parameters of DE and RHC are set as follows: $F = 0.9$, $CR = 0.5$, $NP = 100$, the number of iteration $Nc = 100$, $m = p = 1$, $\boldsymbol{Q} = diag\{1,1,1,1\}$, $T = 1s$. In all experiments, for each UAV, aerodynamic drag $D = 2000$, the thrust $T \in [0,6000]$, the roll angle $\varphi \in \left[-\frac{\pi}{3}, \frac{\pi}{3}\right]$, and UAV's weight $W = 10000$; $D_{safe} = 5$, $D_{com} = 50$.

Given the flight formation has 5 UAVs, they fly as an initial formation shape "|", and the terminal formation is a V-shape formation. Initial states of each UAV are [2,0,0,20], [2,0,0,10], [2,0,0,0], [2, 0, 0, − 10] and [2, 0, 0, − 20]. Desired formation can be described as $\boldsymbol{X}_{ref} = [0, 0, -20, 20; 0, 0, -10, 10; 0, 0, 0, 0; 0, 0, -10, -10; 0, 0, -20, -20]$; choose the UAV-3 as the Leader of the flight formation. In the experiment, after four time horizons, multiple UAVs maneuver to the desired V-shape successfully, and Fig. 5.18 shows the reconfiguration trajectory of multiple UAVs by DE-based RHC controller. Figure 5.19a–d shows the evolution curve of DE algorithm within each time horizon. Figure 5.20 describes the optimal fitness

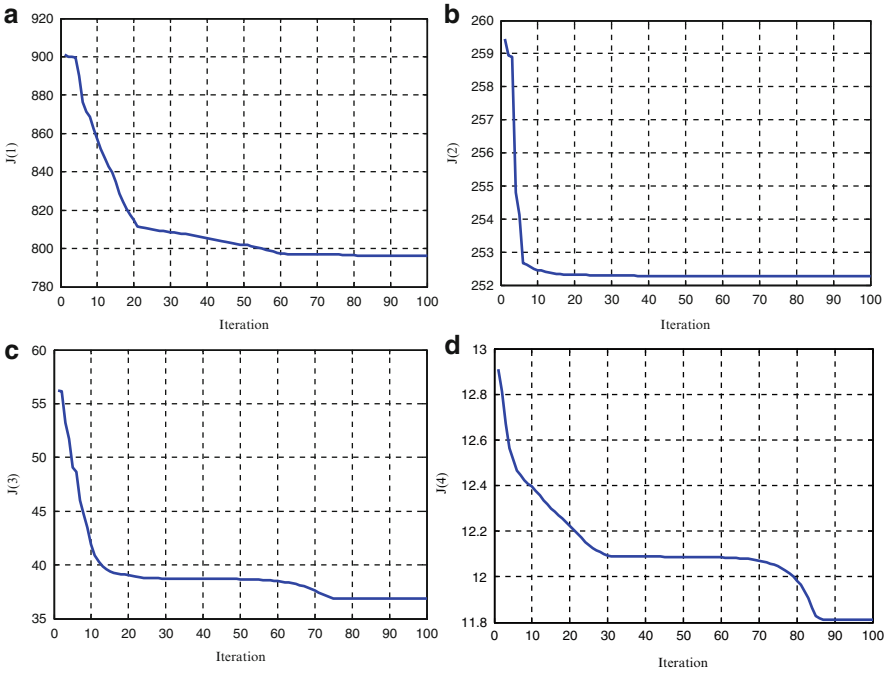

Fig. 5.19 (**a**) Evolution curve at the first time horizon. (**b**) Evolution curve at the second time horizon. (**c**) Evolution curve at the third time horizon. (**d**) Evolution curve at the fourth time horizon (Reprinted from Zhang and Duan (2012), with kind permission from SAGE Publications)

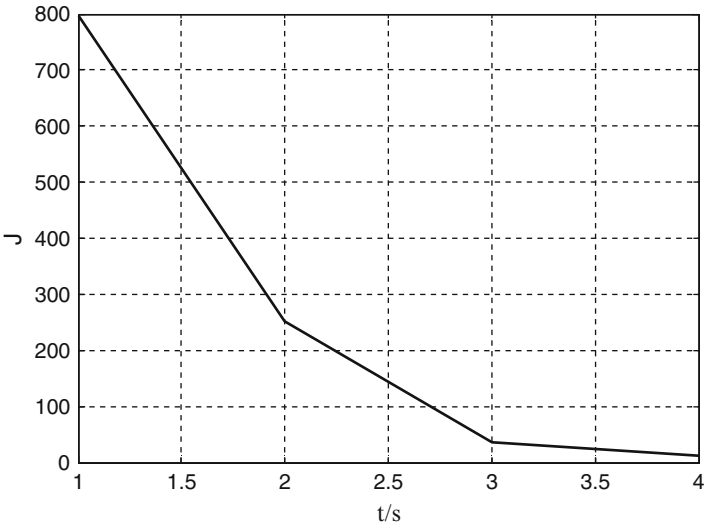

Fig. 5.20 Fitness function value (Reprinted from Zhang and Duan (2012), with kind permission from SAGE Publications)

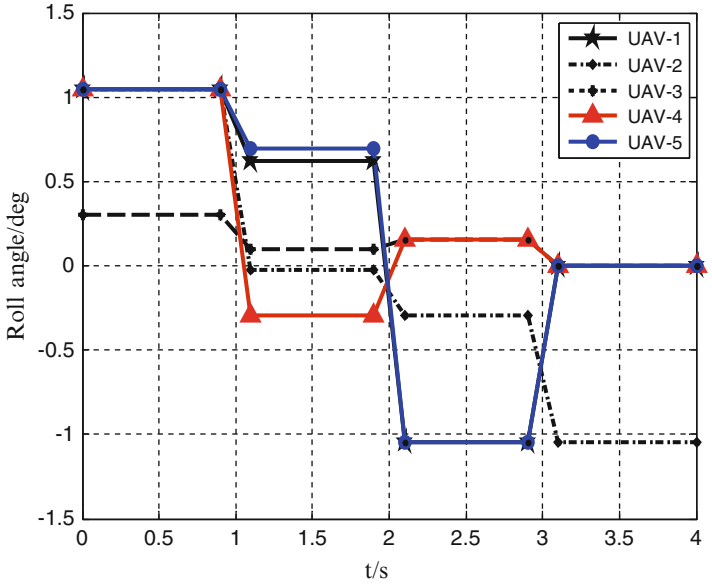

Fig. 5.21 Roll angle at every time horizon (Reprinted from Zhang and Duan (2012), with kind permission from SAGE Publications)

value at each time horizon. Figures 5.21 and 5.22 show the optimal control actions implemented to each UAV, including the thrust and the roll angle. Figure 5.23 shows the distance between two UAVs, which is less than the communication distance and greater than safe anti-collision distance.

Another simulation is as follows. Initial states of each UAV are set as [2,π,0,20], [2,π,0,10], [2,π,0,0], [2, π, 0, − 10], and [2, π, 0, − 20]. Still choose the UAV-3 as the Leader, and the desired formation is $\boldsymbol{X}_{ref} = [0, 0, -20, 20; 0, 0, -10, 10; 0, 0, 0, 0; 0, 0, -10, -10; 0, 0, -20, -20]$, which is also a V-shape formation. Figures 5.24, 5.25, 5.26, 5.27, and 5.28 show the reconfiguration results after five time horizons.

From these experiment results, it is obvious that our proposed DE-based RHC controller can solve the multiple UAV formation reconfiguration problem efficiently.

5.5 Conclusions

This chapter deals with three significant problems in the multiple UAV formation flight problem, which are respectively formation control, close formation (tight formation), and formation configuration.

In Sect. 5.2, a chaotic PSO-based nonlinear dual-mode RHC method is proposed for solving the constrained nonlinear systems. The presented chaotic PSO derives

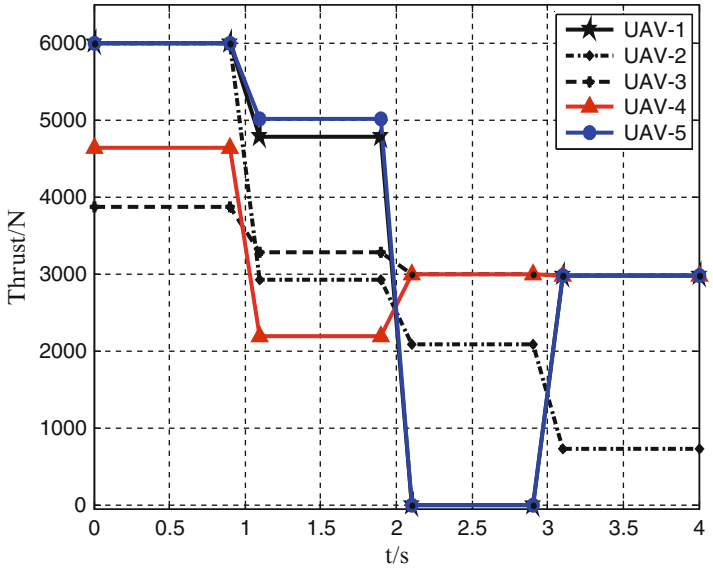

Fig. 5.22 Thrust at every time horizon (Reprinted from Zhang and Duan (2012), with kind permission from SAGE Publications)

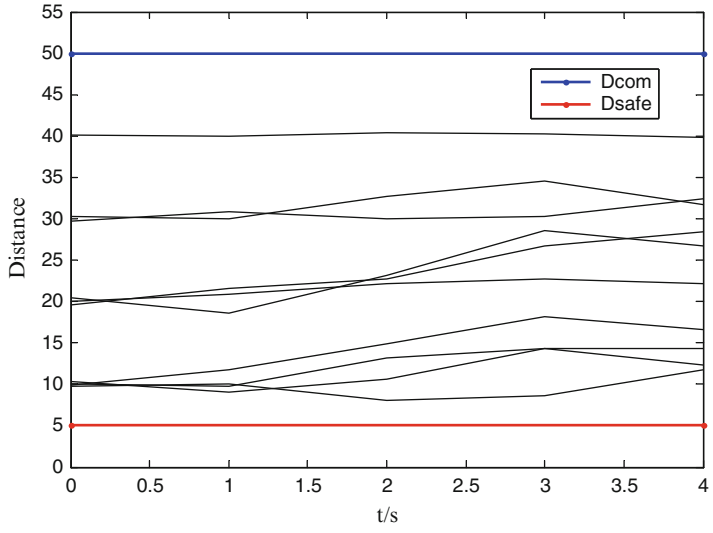

Fig. 5.23 Distance between UAVs (Reprinted from Zhang and Duan (2012), with kind permission from SAGE Publications)

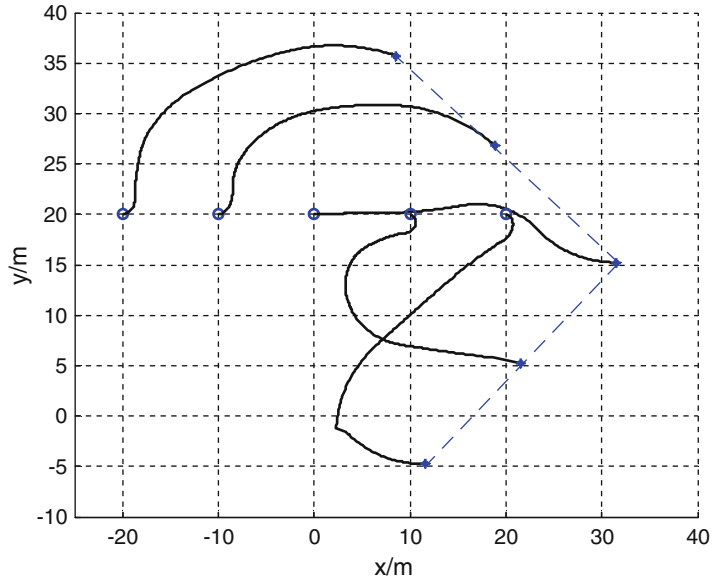

Fig. 5.24 Reconfiguration trajectory of multiple UAVs; "o" is the initial position, and "•" is the terminal position (Reprinted from Zhang and Duan (2012), with kind permission from SAGE Publications)

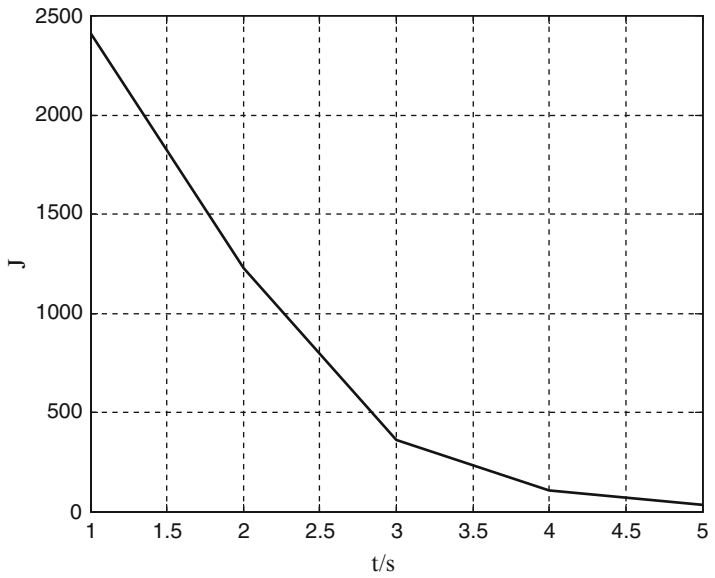

Fig. 5.25 Fitness function value (Reprinted from Zhang and Duan (2012), with kind permission from SAGE Publications)

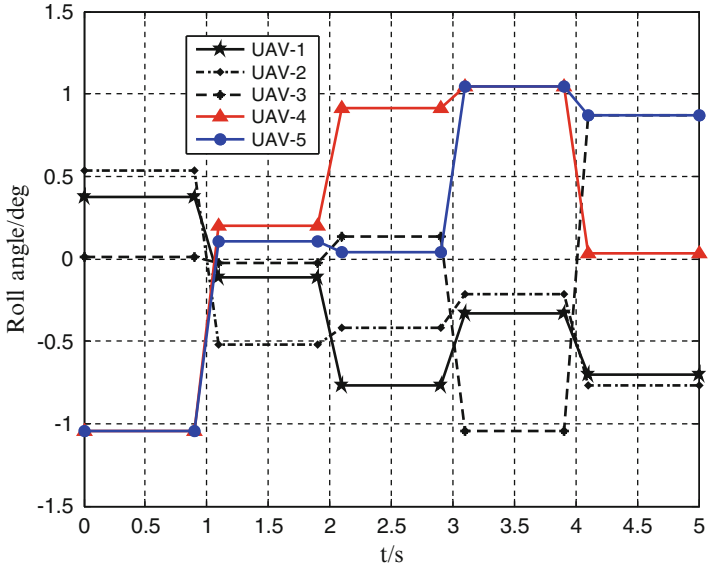

Fig. 5.26 Roll angle at every time horizon (Reprinted from Zhang and Duan (2012), with kind permission from SAGE Publications)

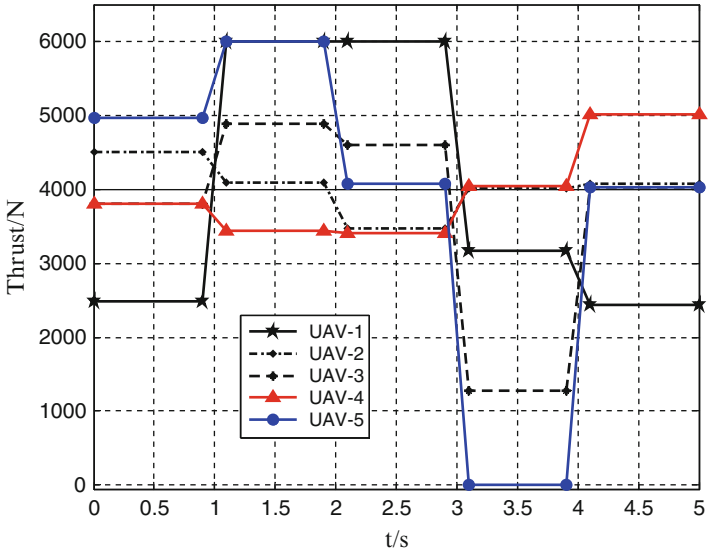

Fig. 5.27 Thrust at every time horizon (Reprinted from Zhang and Duan (2012), with kind permission from SAGE Publications)

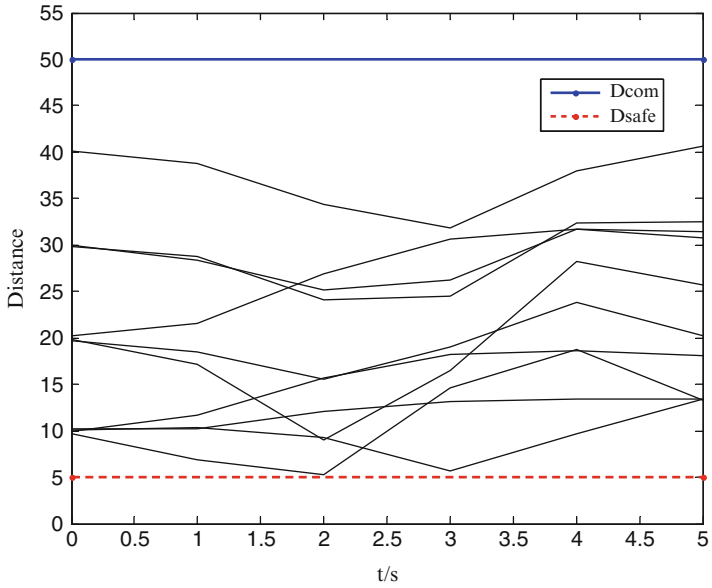

Fig. 5.28 Distance between UAVs (Reprinted from Zhang and Duan (2012), with kind permission from SAGE Publications)

both formation model and its parameter values, and the control sequence is predicted in this way, which can also guarantee the global convergence speed. A dual-model control strategy is used to improve the stability and feasibility for multiple UAV formation flight controller, and the state-feedback control is also adopted, which model is based on the invariant set theory. Then a novel type of control strategy of using hybrid RHC and DE algorithm is proposed based on the nonlinear model of multiple UAV close formation in Sect. 5.3. The issue of multiple UAV close formation is transformed into several online optimization problems at a series of receding horizons, while the DE algorithm is adopted to optimize control sequences at each receding horizon. Moreover, based on the Markov chain model, the convergence of DE is proved. The working process of RHC controller is presented in detail, and the stability of close formation controller is also analyzed. The formation configuration, which is about diving multiple UAVs to form a new flying formation state, is explained in detail using the DE-based RHC in Sect. 5.4. The global control problem of multiple UAV formation reconfiguration is transformed into several online local optimization problems at a series of receding horizons, while the DE algorithm is adopted to optimize control sequences at each receding horizon. Both the feasibility and effectiveness of these three proposed methods are verified by series of experiments.

References

Binetti P, Ariyur KB, Krstic M, Bernelli F (2003) Formation flight optimization using extremum seeking feedback. J Guid Control Dyn 26(1):132–142

Duan H, Liu S (2010) Non-linear dual-mode receding horizon control for multiple unmanned air vehicles formation flight based on chaotic particle swarm optimisation. IET Control Theory Appl 4(11):2565–2578

Duan H, Ma G, Luo D (2008) Optimal formation reconfiguration control of multiple UCAVs using improved particle swarm optimization. J Bionic Eng 5(4):340–347

Duan H, Zhang Y, Liu S (2011) Multiple UAVs/UGVs heterogeneous coordinated technique based on Receding Horizon Control (RHC) and velocity vector control. Sci China Technol Sci 54(4):869–876

Duan H, Luo Q, Ma G, Shi Y (2013a) Hybrid particle swarm optimization and genetic algorithm for multi-UAVs formation reconfiguration. IEEE Comput Intell Mag 8(3):16–27

Duan H, Luo Q, Yu Y (2013b) Trophallaxis network control approach to formation flight of multiple unmanned aerial vehicles. Sci China Technol Sci 56(5):1066–1074

Dunbar WB, Murray RM (2006) Distributed receding horizon control for multi-vehicle formation stabilization. Automatica 42(4):549–558

Giulietti F, Pollini L, Innocenti M (2000) Autonomous formation flight. IEEE Control Syst 20(6):34–44

Hendrickx JM, Fidan B, Yu C, Anderson BD, Blondel VD (2008) Formation reorganization by primitive operations on directed graphs. IEEE Trans Autom Control 53(4):968–979

Kwon WH, Han SH (2005) Receding horizon predictive control: model predictive control for state models. Springer, New York

May RM (1976) Simple mathematical models with very complicated dynamics. Nature 261(5560):459–467

Pachter M, D'Azzo JJ, Proud AW (2001) Tight formation flight control. J Guid Control Dyn 24(2):246–254

Price K, Storn R (1997) Differential evolution–a simple evolution strategy for fast optimization. Dr Dobb's j 22(4):18–24

Proud AW, Pachter M, D'Azzo JJ (1999) Close formation flight control. Air Force Inst of Tech Wright-Patterson AFB OH School of Engineering, Ft. Belvoir Defense Technical Information Center

Shi Y, Eberhart R (1998) A modified particle swarm optimizer. In: Proceedings of the 1998 IEEE International Conference on Evolutionary Computation (IEEE World Congress on Computational Intelligence), Anchorage, AK, 1998. IEEE, pp 69–73

Stipanović DM, Inalhan G, Teo R, Tomlin CJ (2004) Decentralized overlapping control of a formation of unmanned aerial vehicles. Automatica 40(8):1285–1296

Ueno S, Kwon SJ (2007) Optimal reconfiguration of UAVs in formation flight. In: Proceedings of 2007 International Conference on Instrumentation, Control, Information Technology and System Integration (SICE, 2007 annual conference), Takamatsu. IEEE, pp 2611–2614

Wang X, Yadav V, Balakrishnan S (2007) Cooperative UAV formation flying with obstacle/collision avoidance. IEEE Trans Control Syst Technol 15(4):672–679

Zelinski S, Koo TJ, Sastry S (2003) Optimization-based formation reconfiguration planning for autonomous vehicles. In: Proceedings of IEEE International Conference on Robotics and Automation (ICRA'03), Taipei. IEEE, pp 3758–3763

Zhang X, Duan H (2012) Differential evolution-based receding horizon control design for multi-UAVs formation reconfiguration. Trans Inst Meas Control 34(2–3):165–183

Zhang X, Duan H, Yu Y (2010) Receding horizon control for multi-UAVs close formation control based on differential evolution. Sci China Inf Sci 53(2):223–235

Zhang Y, Duan H, Zhang X (2011) Stable flocking of multiple agents based on molecular potential field and distributed receding horizon control. Chin Phys Lett 28(4):040503